Multidisciplinary Coupling for Hybrid-Electric Aircraft Design and Strategic Airline Planning Including Off-Design Performance

Coelho Antunes, S.; Proesmans, P.; Santos, Bruno F.; Hoogreef, M.F.M.; Birolini, Sebastian

DOI
10.2514/6.2025-2375

Publication date
2025

Document Version
Final published version

Published in
Proceedings of the AIAA SCITECH 2025 Forum

AIAA SciTech Forum
6-10 January 2025, Orlando, FL
AIAA SCITECH 2025 Forum

10.2514/6.2025-2375

Multidisciplinary Coupling for Hybrid-Electric Aircraft Design and Strategic Airline Planning Including Off-Design Performance

Sofia Coelho Antunes*, Pieter-Jan Proesmans†, Bruno F. Santos‡ and Maurice F. M. Hoogreef§
Delft University of Technology, P.O. Box 5058, 2600GB Delft, The Netherlands

Sebastian Birolini¶
University of Bergamo, Via 7 Pasubio 7b, 24044, Dalmine (BG), Italy

Hybrid-electric powertrains have shown the potential to reduce aviation climate impact. Since battery capacity is sized for a particular design mission, the emission reduction could be significant when operated at a payload-range combination below the design mission. However, this relation is sensitive to the design point, in particular the design power split ratio and design range. Furthermore, hybrid-electric powertrains would require airlines to adjust their operations. In this study, the interdependencies between hybrid-electric aircraft designs, their off-design performance, and the network's performance are evaluated. The effect of modifying the design range and the design power split ratio on the aircraft's off-design performance and network performance is evaluated. Several designs are constructed and several operational scenarios are generated. The Air Nostrum network is used as a case study. It is found that when the off-design performance of the hybrid-electric aircraft is considered in the fleet assignment and scheduling of an airline, CO_2 savings equal to 15% can be attained while incurring a minimal loss in profit of 1.35%. This research highlights how modifying the design range of hybrid-electric aircraft has a larger impact on the applicability of the former in regional airline networks than the modification of the design power split ratio.

Nomenclature

OD	Origin-Destination
AR	Aspect Ratio [-]
CASK	Cost Available Seat Kilometer [€/km]
ICAO	International Civil Aviation Organization
LD	Landing Distance [m]
LF	Load Factor [-]
MTOM	Maximum Take-off Mass
OEI	One Engine Inoperative
PMAD	Power Management and Distribution
RASK	Revenue Available Seat Kilometer [€/km]
SOC	State of Charge [%]
TOL	Take-off Length [m]
C_e	Cost per emission [€/ton]
g	Gravitational acceleration [m/s^2]
η	Efficiency [-]
γ	Flight path angle [deg]
ϕ	Supplied power split ratio [-]
Π	Pressure ratio [-]
φ	Shaft power ratio [-]
$\dot{m}$	Mass Flow [kg/s]
UT_{max}	Maximum allowable aircraft utilization [h]
C	Work Interaction coefficient [-]
$c_{ownership}$	Aircraft ownership cost [€]
C_D	Drag coefficient [-]
C_L	Lift coefficient [-]
C_{D0}	Zero-lift drag coefficient [-]
c_{pt}	Turbine's specific heat at constant pressure [J/kg K]
D	Drag force [N]
E	Energy consumed [J]
e	Oswald efficiency factor [-]
e_{bat}	Specific energy battery (pack) [Wh/kg]
e_f	Specific energy fuel [Wh/kg]

*MSc. Graduate, Faculty of Aerospace Engineering
†Assistant Professor, Faculty of Aerospace Engineering, AIAA Member
‡Associate Professor, Faculty of Aerospace Engineering
§Assistant Professor, Faculty of Aerospace Engineering, AIAA Senior Member, m.f.m.hoogreef@tudelft.nl
¶Assistant Professor, Department of Management, Information and Production Engineering

e_l	CO_2 emissions on flight leg l [kg]
ep_{bat}	Specific power battery (pack) [Wh/kg]
h	Altitude [m]
hs	Specific enthalpy [J/kg]
L	Lift force [N]
M	Mach number [-]
m	Mass [kg]
n	Propeller number [-]
P	Power [W]
P_{specific}	Specific power [J/kg]
P_p	Total powertrain power [W]
R	Range [m]
T	Thrust Produced [N]
T_{specific}	Specific thrust [Ns/kg]
$T_{t,4.5}$	Total temperature before the power turbine [K]
$T_{t,4}$	Turbine inlet temperature [K]
$T_{t,5}$	Total temperature after the power turbine [K]
u	Direct passengers [-]
V	Velocity [m/s]
W/P	Power loading [N/W]
W/S	Wing loading [N/m^2]
W	Weight [N]
w	Transfer passengers [-]
w_e	Emissions objective function weight [-]
W_l	Flight leg weight [€]
w_p	Profit objective function weight [-]
bt	Block time [h]
CDemand	Constrained demand [-]
UDemand	Unconstrained demand [-]
0	Engine station zero
f	Fuel/Kerosene
$p1$	Propeller 1
$p2$	Propeller 2
$s1$	Primary powertrain
$s2$	Secondary powertrain
app	Approach phase
bat	Battery
buffet	Buffet phenomena
cruise	Cruise phase
design	Design conditions
em1	Electric motor 1
em2	Electric motor 2
gb	Gearbox
gt	Gas turbine
pay	Payload

I. Introduction

Market forecasts from *Boeing*[a] and *Airbus*[b] estimate that this prosperity may mean a yearly growth of up to 3.8 % in the period between 2022 and 2041. In light of the recent ambitious climate goals set by the *United Nations*[c], one of the greatest challenges is maintaining the balance between profitability and sustainability.

Generally speaking, lowering the amount of fuel consumed directly correlates to lowering the amount of emissions produced. Hence, numerous attempts have been made around electrified powertrains. However, one of the largest obstacles to electric flight is achieving a viable and safe specific energy density to cover enough profitable routes. [1] Due to this limitation, electric aircraft would most likely be restricted to regional operations with a challenge lying in particular in reserve energy requirements. Clean sheet designs using a combustible reserve energy supply promise design ranges of up to 1000km [2] for competitive payloads.

Hybrid-electric (HE) aircraft on the other hand, use both a battery and a combustible energy carrier for normal operations. In addition to providing more flexibility, the hybrid design provides designers with an additional degree of freedom and design variable: the supplied power split ratio [3]. This variable controls the split between the power which is provided by the battery and the power which is provided by the fuel at every moment during the mission. The interplay between power split ratio and fuel savings is not straightforward. *Hoogreef et al.* [4] concluded that on-design fuel savings highly depend on the combination of design range and design supplied power split ratio. Large design ranges, imply a large battery and thus incur a weight penalty which is not compensated by the hybrid powertrain. Although it may be that at the design point, fuel savings do not occur, *Bonnin & Hoogreef* [5] have demonstrated that at off-design conditions (smaller mission length and smaller payload), the amount of fuel saved is significant. For an

[a] `https://www.boeing.com/commercial/market/commercial-market-outlook/index.page` - visited: May 2023

[b] `https://www.airbus.com/en/products-services/commercial-aircraft/market/global-market-forecast` - visited: May 2023

[c] `https://www.un.org/en/climatechange/paris-agreement` - Visited: May 2023

aircraft carrying 70 passengers with a design range around 900 km and a design cruise power split ratio equal to 10%, when flying a mission with a length of around 500 km at maximum payload the fuel consumed decreases by up to 25%. The authors attribute this benefit to the ability to increase the supplied power split ratio during cruise to values well above the design value. Moreover, this study, in addition to [2], has shown that the relative performance of various design comparisons to kerosene aircraft is insensitive to the design payload - in sharp contrast to the sensitivity to design range and power split ratio.

Furthermore, the operational context in which aircraft are used has a significant impact on the block emissions. Moreover, deciding the type of missions a certain aircraft flies is part of airlines' strategic planning phase. This would also be the time to consider novel technologies, such as electrified powertrains, and the challenges they bring about (e.g. longer turnaround times). The aircraft's performance and characteristics highly influence the choices an airline can make. More often than not the characteristics of the available aircraft do not exactly serve a certain network and thus the aircraft end up operating at a sub-optimal level and thus have a larger environmental impact [6]. There is therefore a need to follow a systems-of-systems approach in which aircraft design and their operations are considered simultaneously. Several researchers have built frameworks which study the coupling and the interdependencies between aircraft design and an airline network. *Taylor & Weck* [7] were leaders in adopting this perspective on the aviation system. Shortly after, *Jansen & Perez* [8] created a framework which couples aircraft design optimization with their allocation to routes in an operator's network. Moreover, *Roy et. al* [9], developed a framework which couples aircraft design with fleet allocation while maximizing profit. Note that, the aforementioned studies share two common aspects: only consider profit as the optimization objective and only consider conventional aircraft.

Recently, attention turned to novel aircraft technologies. *Scheers* [10], connected a fleet-and-network allocation model (based on the model by *Zuijderwijk* [11]) to a hybrid-electric conceptual design tool and optimized the fleet composition based on the total airline profit. Additionally, hybrid-electric aircraft were separately redesigned for minimum CO_2 emissions. This was accomplished by enabling adjustments to the cruise velocity, cruise altitude, and cruise supplied power split ratio. Modifying these parameters led to a significant decrease in network CO_2 emissions without a significant penalty in terms of profit. This demonstrates the impact that these design variables have on the environmental impact of hybrid-electric aircraft. Furthermore, in the CHYLA project[d], dynamic programming was used to create an airline's schedule and fleet assignment while considering both conventional and hybrid-electric aircraft[4]. Dynamic programming has been used to simultaneously solve the timetable design and fleet assignment problem [12, 13].

Several researchers have followed a systems-of-systems approach and have created frameworks which allow for the study of the interdependencies between aircraft design and their operational environment. This research domain has even been extended to hybrid-electric aircraft in which these were allocated to routes based purely on profit. Furthermore, hybrid-electric aircraft have shown to bring benefits when operated outside their design point and additionally, their environmental impact can be minimized by finding a suitable design cruise altitude-velocity-power split combination. Nevertheless, no framework has been created which allows studying the potential implications of operating hybrid-electric aircraft outside their design point on an airline network. This may shed light on how these aircraft can be made better suited for operating a certain network in terms of both profit and environmental impact.

From literature, three variables, were identified to have the largest effect on a hybrid-electric (HE) aircraft's performance. Two variables are aircraft design related: the design range and the design power split ratio; while a third is also related to how the aircraft is operated: cruise speed. With a focus on these three variables, the current work aims to understand how they affect the off-design performance of a HE aircraft and in turn, how these modifications affect the performance of an airline network which includes these aircraft. To this end, the current work proposes to quantify the off-design performance by exploring the payload-range performance for different cruise velocities of several conceptual designs of hybrid-electric aircraft. These are then integrated in a fleet assignment and scheduling model which makes use of dynamic programming to select the best schedule which maximizes an objective function.

This paper first describes the overall framework setup, aircraft sizing methods, fleet assignment, and coupling strategy in section II. section III provides the details of the case study and treats the verification of fleet assignment and scheduling module. Subsequently, section IV presents and discusses the results. Finally, important conclusions are gathered in section V.

[d]CHYLA - Credible HYbrid eLectric Aircraft `https://cordis.europa.eu/project/id/101007715`

II. Methodology

The framework is split into three separate parts: the *Hybrid-Electric Aircraft Design Module*, the *Off-design Analysis Module* and the *Fleet Assignment and Scheduling Module*. A description of the methodology followed can be found in Sections II.A, II.B and II.C, respectively. Furthermore, given the interdependencies between aircraft design and the operational environment in Section II.D a description of the coupling strategy adopted is given.

A. Hybrid-Electric Aircraft Design Module

The first element in the framework is the hybrid-electric aircraft conceptual design module, developed by *Proesmans & Vos*[14]. However, the work described in the following subsections is an extension to this by *Scheers*[10] to design hybrid-electric aircraft. This extension used the methodology developed by *de Vries* [3] to model hybrid-electric powertrains and a simplified mission analysis using a equation for hybrid-electric aircraft [15]. Given the objective of the current work, the fidelity and accuracy had to be increased. This entails further detailing the powertrain system behavior under different conditions. This allows for the implementation of a more detailed mission analysis, which can also assess the off-design performance of hybrid-electric aircraft. These modifications implemented are highlighted.

1. Module Structure

The structure of the hybrid-electric aircraft design module can be seen in Figure 1. Similarly to the framework developed by *Scheers*, top-level requirements: design range (R_{design}), payload mass (m_{pay}), take-off length (TOL), approach speed (V_{app}), cruise speed (V_{cruise}) and cruise altitude (h_{cruise}); are used once to run the *Initializer*, which, provided with a design mission profile, design payload mass and aircraft type (e.g. turboprop), creates a first estimate of the mass breakdown and the aerodynamic performance of a conventional kerosene aircraft. This is based on statistical Class I weight and aerodynamic data[16]. The largest changes were made within the *Synthesizer*, which is responsible for conceptually designing a hybrid-electric aircraft. This composed of a power-loading and powertrain model, geometry estimation, a class II weight estimation and a mission analysis. The Class II weight estimation submodule was kept as implemented by *Scheers*[10].

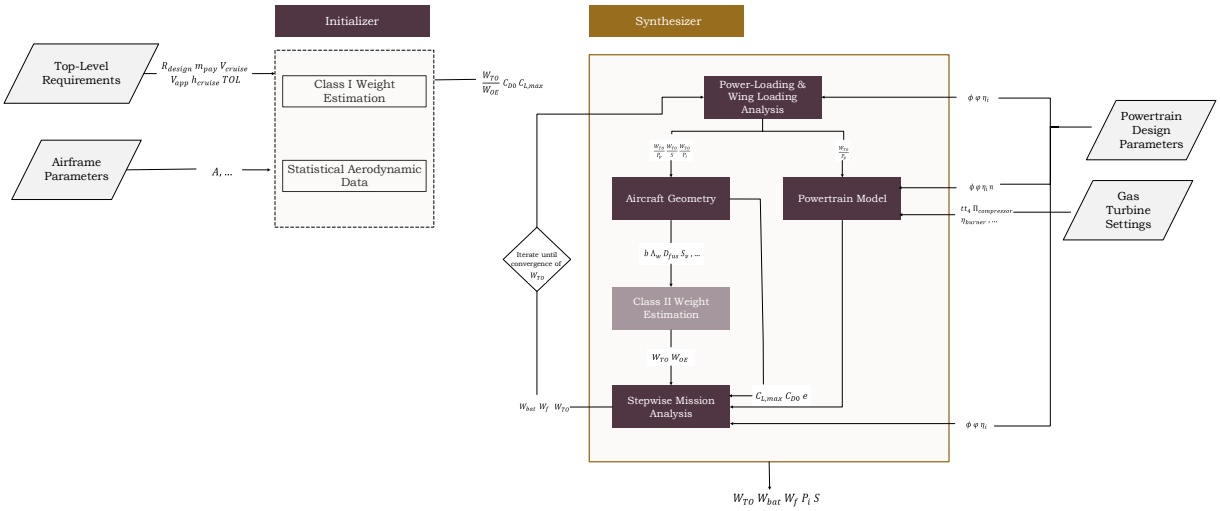

Fig. 1 Schematic of the Hybrid-Electric Aircraft Design Module Framework

2. Power Loading Diagram

The first discipline within the *Synthesizer* is the power-loading diagram. Here, a constraint analysis is performed to determine the hybrid aircraft power-loading (W/P) and wing-loading (W/S) from top-level requirements: take-off distance, stall speed, approach speed, cruise speed and climb gradients in one engine inoperative (OEI) conditions.

3. Aircraft Geometry

The aircraft geometry submodule estimates a preliminary aircraft geometry, used to update the aircraft aerodynamic parameters (C_D, C_{D0} and e) following the method of *Obert* [17]. The aircraft sizing follows the method by *Torenbeek* [18], whereas the turboprop dimensions are based on the work of *Thijssen* [19]. A constraint of 36m is enforced on the wingspan[e], as well as a constraint on maximum allowable cruise lift coefficient [20].

Fuel Tank Volume

In order to determine the battery location, a preliminary estimate of the maximum fuel which can be contained in the wings is required. An estimate for the span occupied by the fuel tanks and the wing area occupied by the fuel tanks was used, following a adaptation of the method detailed by Torenbeek [18] with the following assumptions into account:

- Fuel tank is split in a center tank (inside the fuselage) and a main tank (outside the fuselage).
- The main tank starts at the intersection with the fuselage and ends at 85 % of the semi-span.
- The main tank and the center tank are assumed to be located between the front and rear spar, assumed at 15% and 75% of the local chord, respectively [18].
- The existence of a kink is taken into account by assuming the main wing to be made of two trapezoids.

Battery Location

It is assumed that the aircraft has only one battery compartment, either in the fuselage or inside the wing. When this is located inside the wing, it is assumed that this is only possible in the portion of the wing inside the fuselage (i.e. the center tank). In case the center tank volume is larger than the required battery volume, the remainder is assumed to be used to store fuel. In case the center tank is not large enough, it is assumed that the battery must be fully stored in the fuselage. Consequently, the entire tank volume inside the wing (center and main tank) is assumed to be able to store fuel. Two safety factors are added to the battery volume: a factor of 1.2 to account for cables and a factor of 1.1 is added to account for the fact that the battery is a solid block and hence some places would not be properly occupied by it [10].

4. Powertrain Model & Design

To get a more accurate indication of how a hybrid-electric powertrain would perform at each mission stage, the powertrain model and design submodule should be able to, given certain flight conditions, (1) determine how much fuel and battery energy is being consumed and (2) it should be able to model the energy and power flow within a hybrid powertrain. To achieve these two characteristics, two models were combined. A turboprop engine cycle analysis tool [19] and a hybrid powertrain model[3]

Hybrid Powertrain

Following the approach by *de Vries* [3], the powertrain is modeled by a series of simple constituents, namely: energy sources, subcomponents and power and energy paths. Cables, switches and other smaller components are gathered in a power management and distribution box (PMAD), which similar to other electrical subcomponents is also characterized by a efficiency, specific energy and specific power.

An example of the powertrain model for a parallel-hybrid architecture as used in the present study can be seen in Figure 2. Each component transmits a certain amount of power to the adjacent components, where the direction of the power flows is determined by the operating mode. For the present work, the only operating mode considered was the fourth operating mode detailed by *de Vries* [3]. This mode is characterized by the fact that the power provided to the propeller comes from the electric motor and the gas turbine.

To attain the powers flowing from and into each subcomponent in the powertrain, a system of equations is solved while attending not only, to the subcomponent efficiencies but also by power control parameters. In this case, the supplied power ratio (Equation 1) and gas turbine throttle. The supplied power ratio (ϕ) specifies the split between how much of the system's power is provided by the battery (P_{bat}) and how much is supplied by the fuel (P_f). Additionally, a shaft power ratio (φ) may specify the amount of shaft power of a secondary power path, with respect to the total shaft power produced in case of distributed propulsion. (For the present parallel hybrid, this is set to zero).

$$\phi = \frac{P_{\text{bat}}}{P_{\text{bat}} + P_f} \tag{1}$$

$$\varphi = \frac{P_{s2}}{P_{s2} + P_{s1}} \tag{2}$$

[e] `https://skybrary.aero/articles/icao-aerodrome-reference-code` [Accessed: 05/11/2023]

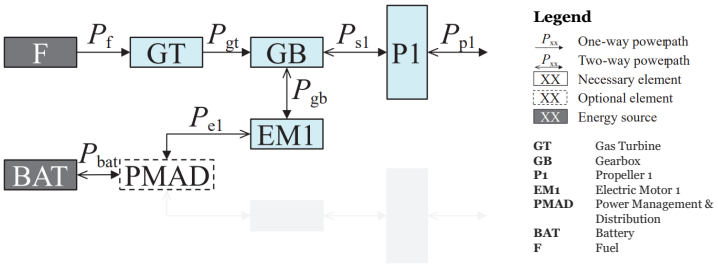

Fig. 2 Example of parallel hybrid architecture [3]

Turboprop Engine Cycle Analysis

A turboprop engine cycle analysis method is used to design and analyze a gas turbine at on- and off-design conditions. The turboprop engine cycle analysis was implemented based on the method developed by *Mattingly et al.* [21]. Given certain atmospheric conditions and several design variables which are summarized in Table 12 in Appendix A, the thrust (T), the specific power (P_{specific}) and the specific thrust (T_{specific}) are computed and used to quantify the design air mass flow ($\dot{m}_0$) and the design power consumed (P_{design}), according to Equation 3 and Equation 4, respectively.

$$\dot{m}_0 = \frac{1.1T}{T_{\text{specific}}} \tag{3}$$

$$P_{\text{design}} = \dot{m}_0 \cdot P_{\text{specific}} \tag{4}$$

The aforementioned parameters are determined based on a non-dimensional parameter called the work interaction coefficient (C_{total}). This parameter is defined through Equation 5, where C_{prop} (Equation 6) is the work interaction coefficient of the propeller and C_{core} (Equation 7) is the work interaction coefficient of the core. C_{core} is in general much smaller than C_{prop} since for turboprops, the thrust produced by the core (T_{core}) is much smaller than that produced by the propeller. Furthermore, C_{prop} depends on the propeller efficiency η_{prop} and the shaft power provided to the propeller (P_s). Both parameters are normalized with respect to the air mass flow and the specific enthalpy of the air (hs_0).

$$C_{\text{total}} = C_{\text{prop}} + C_{\text{core}} \tag{5}$$

$$C_{\text{prop}} = \frac{\eta_{\text{prop}} \cdot P_s}{\dot{m}_0 \cdot hs_0} \tag{6}$$

$$C_{\text{core}} = \frac{T_{\text{core}} \cdot V_0}{\dot{m}_0 \cdot hs_0} \tag{7}$$

Coupling of Models

As previously mentioned, for the parallel hybrid electric aircraft, the power provided to the propeller is generated by both the gas turbine and the electric motor, hence P_s of Equation 6 is no longer only dependent on the work performed by the power turbine. Thus, the shaft power provided to the propeller must comply with Equation 8, where P_{gt} is the power produced by the gas turbine and P_{gb} is the power produced by the electric motor. Note the minus sign, which stems from the sign convention given by *de Vries* 's [3] derivation, where P_{gb} is negative.

$$P_s = \eta_{\text{gb}} \cdot \underbrace{\eta_{mL} \cdot \dot{m}_{4.5} \cdot c_{pt} \cdot (T_{t,4.5} - T_{t,5})}_{P_{\text{gt}}} - \eta_{\text{gb}} \cdot P_{\text{gb}} \tag{8}$$

Furthermore, in the approach developed by *de Vries* [3], the powertrain's total output power is known and used to determine all the subcomponent power outputs, including the gas turbine power. In the current work, this no longer applies, since the gas turbine power is computed with the turboprop engine cycle analysis. Hence, an adjustment is made to the system of equations proposed by *de Vries* [3] to determine the battery power, the gearbox power (P_{gb}), and the total powertrain power (P_p), which comply with the selected supplied power ratio, shaft power ratio, and the maximum power that the gas turbine can produce. This is necessary to ensure that the required power equilibrium between the powertrain subcomponents is met. The proposed system of equations can be seen in set of Equations 9. The assumed powertrain properties can be found in Appendix A on Table 13.

$$\begin{bmatrix} -\eta_{gt} & 0 & 0 & 0 & 0 & 0 & 0 & 0 & 0 & 0 \\ 0 & \eta_{gb} & 1 & 0 & 0 & 0 & 0 & 0 & 0 & 0 \\ 0 & 0 & -\eta_{P1} & 0 & 0 & 0 & 0 & 1 & 0 & 0 \\ 0 & -1 & 0 & \eta_{em1} & 0 & 0 & 0 & 0 & 0 & 0 \\ 0 & 0 & 0 & -1 & -\eta_{pmad} & 1 & 0 & 0 & 0 & 0 \\ 0 & 0 & 0 & 0 & 0 & -\eta_{em2} & 1 & 0 & 0 & 0 \\ 0 & 0 & 0 & 0 & 0 & 0 & -\eta_{P2} & 0 & 1 & 0 \\ \phi & 0 & 0 & 0 & (\phi-1) & 0 & 0 & 0 & 0 & 0 \\ 0 & 0 & \varphi & 0 & 0 & 0 & (\varphi-1) & 0 & 0 & 0 \\ 0 & 0 & 0 & 0 & 0 & 0 & 0 & 1 & 1 & -1 \end{bmatrix} \cdot \begin{bmatrix} P_f \\ P_{gb} \\ P_{s1} \\ P_{em1} \\ P_{bat} \\ P_{em2} \\ P_{s2} \\ P_{p1} \\ P_{p2} \\ P_p \end{bmatrix} = \begin{bmatrix} -P_{gt} \\ \eta_{gb} \cdot P_{gt} \\ 0 \\ 0 \\ 0 \\ 0 \\ 0 \\ 0 \\ 0 \\ 0 \end{bmatrix} \tag{9}$$

Off-design Performance

Once the design of the powertrain is complete, its off-design performance can be assessed. Although the power flow within the powertrain is modeled in the same way (with Equation 9), the amount of power that the gas turbine can provided, is determined through the engine cycle analysis[21]. In essence, the gas turbine engine-cycle parameters, determined during the engine sizing, are adjusted by finding the turbine inlet temperature ($T_{t,4}$) and thus fuel mass flow which allows the powertrain to meet either a certain total powertrain power (P_p) or a certain low-pressure spool speed, depending on the mission phase.

5. Mission Analysis

A step-wise approach is adopted in which the instantaneous point performance of the aircraft at discrete time steps is evaluated and used to estimate the battery mass and the fuel mass required to complete the selected mission.

Mission Profile

The design mission profile used was constructed based on several user-specified parameters. These include the rotational speed of the low-pressure spool, the approach speed, the cruise altitude, the cruise speed, the cruise range and the design payload. Furthermore, the design mission was constructed based on the guidelines provided by the *International Civil Aviation Organization* [22]. An example design mission can be observed in Figure 3 and comprises the segments numbered in Table 1 , which can be divided into the following three main stages:

- **A nominal mission**: Aircraft take-off, climb and acceleration until a predetermined cruise altitude and speed. A cruise distance equivalent to the predetermined design range, followed by descend and attempt to land.
- **A reserve mission**: Aircraft diverts to another airport situated at a maximum distance equal to 100nmi, while cruising at an altitude equal to 5000m and speed equal to the nominal cruise speed.
- **Endurance mission:** Aircraft loiters for a total of 30 min at an altitude of 450m above the lading airport.

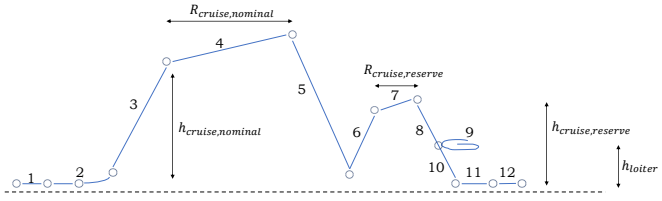

Fig. 3 Example mission profile

Table 1 Mission segments

#	Part	#	Part
1	Start-up and Taxi	7	Cruise 2
2	Take-off	8	Descent 2
3	Climb 1	9	Loiter
4	Cruise 1	10	Descent 3
5	Descent 1	11	Landing
6	Climb 2	12	Taxi & Shutdown

Aircraft State

At each time step the aircraft state is quantified through the equations of motion 10 and 11. It is assumed that the thrust vector is aligned with the flight direction and that the change in flight path angle ($\frac{d\gamma}{dt}$) is equal to zero. Furthermore, a quadratic drag polar is assumed, where the aerodynamic parameters C_{D0} and e are taken from the previously described aerodynamic analysis Section (II.A.3) and used to estimate the aircraft's drag.

$$T - D - W \cdot \sin(\gamma) = \frac{W}{g} \cdot \frac{dV}{dt} \tag{10}$$

$$L = W \cdot \cos(\gamma) \tag{11}$$

Thrust and fuel consumption are quantified through the off-design performance analysis described in Section II.A.4. Depending on the flight phase, either the low-pressure spool speed or the total power the powertrain can produce is

taken to be the constraining factor. For the segments of take-off and climb the former is true, for every other segment the latter applies.

Additionally, since the performance of the aircraft is considered constant over a time step i, the energy drained from the battery and the fuel flow can be computed with Equation 12 and Equation 13, respectively. The power demands at the energy sources (P_{bat} and P_f) are attained from the powertrain model described in Section II.A.4 and the value assumed for the fuel specific energy (e_f) can be found in Appendix A.

$$dE_{\text{bat},i} = P_{\text{bat},i} \cdot dt \tag{12}$$

$$\dot{m}_{f,i} = P_{f,i}/e_f \tag{13}$$

A numerical integration is then used to determine the evolution of the aircraft's state (position, velocity, mass). Equation 14, Equation 15 and Equation 16 are used to compute the horizontal distance (s), the vertical distance (h) and the velocity magnitude (V) at the beginning of the following time step $i+1$, while Equation 17 is used to update the aircraft's mass (m) based on the fuel consumed during the considered time step i.

$$s_{i+1} = s_i + V_i \cdot \cos(\gamma) \cdot dt \tag{14}$$

$$h_{i+1} = h_i + V_i \cdot \sin(\gamma) \cdot dt \tag{15}$$

$$V_{i+1} = V_i + \frac{dV}{dt}_i \cdot dt = a_i \cdot dt \tag{16}$$

$$m_{i+1} = m_i - \dot{m}_{f,i} \cdot dt \tag{17}$$

Finally, the mass of the battery is determined by looking at the total battery energy required to operate the design mission (E_{bat}) and the maximum power the battery must provide ($P_{max,bat}$). If the battery's energy density (e_{bat}) and power density (p_{bat}) are assumed, the mass of the battery (m_{bat}) can be computed with Equation 18 [10]. Note that a minimum state of charge (SOC) of 20% was considered.

$$m_{\text{bat}} = \text{Largest of: } \begin{cases} E_{\text{bat}}/e_{\text{bat}} \cdot (1 + \text{SOC}) \\ P_{\text{max,bat}}/ep_{\text{bat}} \end{cases} \tag{18}$$

Aircraft Emissions

The powertrain emissions were computed by assuming a certain emission index (EI) per combustion subproduct. Furthermore, only CO_2 and NO_x emissions were considered. It was assumed that per kg of fuel burnt 3.16kg of CO_2 would be produced. Moreover, since the emission index of NO_x highly depends on the combustion conditions, the method described by *Dallara* [23] was used.

B. Off-design Analysis Module

Off-design performance analysis implies quantifying the fuel consumption, CO_2 and NO_x emissions for different payload-range combinations. To achieve this a stepwise mission analysis is used according to the method detailed in Section II.A.5. In order to limit the computational time, only the nominal mission was evaluated for each payload-range combination and the reserve values (fuel consumed, CO_2 and NO_x emitted) were assumed to be equal to those of the design mission.

1. Hybrid-Electric Aircraft

Assuming a fully-charged battery before every flight, a hybrid-electric aircraft always contains the same battery energy, regardless of mission range and mission payload. Hence, as demonstrated by *Bonnin & Hoogreef* [5], for shorter ranges and lighter payloads, the supplied power split during cruise can increase with respect to the design mission. Thus, relatively more battery energy is used and less fuel is required.

A payload-range sweep is performed for various off-design missions to determine: the fuel consumed, CO_2 and NO_x emissions produced and the maximum viable supplied power split in cruise. Special attention was given to the gas turbine's operational limits. Beyond a certain supplied power split, the power required from the gas turbine is so little with respect to its design power, that the gas turbine can no longer physically operate under those conditions. Hence, the maximum feasible supplied power split in cruise is limited by both the battery energy content but also by the gas turbine's operating envelope.

2. Mach Number Variation

In addition to exploring the payload-range limits, also the effect on payload-range performance depending on cruise Mach number is studied. This variation was attained by varying the cruise velocity and maintaining the cruise altitude constant. Three different cruise Mach numbers were considered: below the design value, at the design value and above the design value. Ultimately, the goal is to attain, for each cruise velocity considered, a 2D interpolated function, which, if provided with a payload-range combination, is able to output the fuel consumed, the CO_2 and NO_x produced and, for hybrid-electric aircraft, the maximum viable cruise power split.

C. Fleet Assignment and Scheduling Module

This modules produces a weekly schedule for an airline, assigns aircraft to specific flights and determines the best cruise speed for each flight. It takes inputs related to the airport network, including details on their location, runway length, demand between any pairs of airports and performance of all aircraft to be considered (both on- and off-design). Once a database of aircraft sized with the method detailed in Section II.A is created and their off-design performance has been explored (following Section II.B), the aircraft can be embedded in a simulated network environment. The modeling of this environment is detailed in the following subsections.

During the modeling process, several assumptions were made for the fleet assignment and scheduling module:

- All airports have recharging stations.
- An operational day starts at 6:00am and ends at 00:00pm UTC.
- Aircraft is always able to land at the largest available runway.
- The electricity price is assumed to be equal to 0.1445 €/kWh [11].
- The fuel price is assumed to be equal to 0.8 €/kg (0.067€/kWh)[11].
- Turnaround time is considered to be equal to 45 min for hybrid aircraft and 30 min for conventional aircraft.
- Battery is always fully charged before each flight.
- Hybrid aircraft ownership cost is assumed to be 20% larger than their conventional equivalent. The assumption is based on the purchasing price difference between electric cars and conventional cars.[f]
- Transfer passengers do not have a preference for the amount of transfer time they are to spend at the hub.
- Demand attraction band is considered to be equal to 1 hour, meaning we assume passengers can be served within one hour of their preferred departure time.
- The cost of CO_2 is set at €80/ton emitted. This follows European emission trading scheme prices. [g]
- Network is modeled to be a hub-and-spoke network with one hub.
- The overnight airport is not necessarily the hub. If not the hub, no overnight parking fee is considered.

1. Module Structure

The logic and the flow of information within the *Fleet Assignment and Scheduling Module* is visualized in Figure 4. It requires three distinct types of data: demand data, aircraft data and airport data. Demand data specifies the number of passengers desiring to fly between two specific airports. Details regarding the processing and modeling of demand can be found in Section II.C.4. Aircraft data comprises information regarding on- and off-design performance of each aircraft considered. Airport data includes which airports are to be considered, their runway lengths and whether or not they are operational hubs.

Dynamic programming was selected to solve the integrated fleet assignment and scheduling problem. This approach is an optimization method which separates a large complex problem into smaller sub-problems which can be solved individually and only once, thus avoiding redundant computations [24]. For the current work, the complex problem to be solved consists of constructing an airline fleet and its weekly schedule while maximizing profit and/or minimizing CO_2 emissions. Solving a sub-problem implies creating the weekly schedule of a single aircraft. All sub-problems are solved in parallel to reduce computational time. Once all the sub-problems have been solved, the aircraft **a** with the largest objective function value is selected and added to the fleet, and its served demand is subtracted from the remaining total. The details of the objective function used for the iterative fleet selection can be found in Section II.C.3. This process is repeated until it is either not profitable to add a new aircraft or demand has been served entirely. Note that per iteration there are **m** sub-problems to be solved, where **m** is equal to the number of aircraft types in the database.

[f] `https://www.hdfcergo.com/blogs/car-insurance/electric-cars-vs-petrol-cars`[Accessed: 12/12/2023]

[g] `https://ember-climate.org/data/data-tools/carbon-price-viewer/` [Accessed: 12/12/2023]

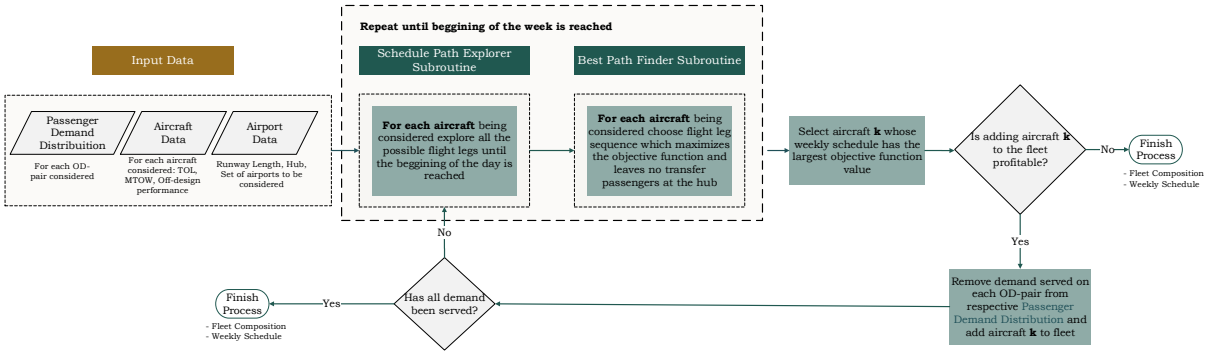

Fig. 4 Fleet Assignment and Scheduling Module flowchart

2. Schedule Synthesizer

The process of creating the weekly schedule for an aircraft is composed of two main elements: the **Schedule Path Explorer** and the **Best Path Finder**. These are performed in sequential order, for each day of the week.

Schedule Path Explorer

The Schedule Path Explorer considers one day at a time and examines the demand between each airport in the network at a certain time t during the day, the profit that can be attained and the CO_2 emissions produced for each specific flight. Its objective is to explore all possible schedule combinations for a specific aircraft in a single day. By starting at the end of the day and progressively moving towards the beginning of the day, at each time step t, the algorithm explores all possible actions within the *action space* (set of actions possible at a certain state). It first determines whether to fly to another airport or to stay at the current airport for next time step. In case it chooses to fly to another airport, the algorithm can explore the possibility of cruising at different cruise velocities.

To capture the spatial and temporal complexity of the problem, a *time-space network* was used. This has two dimensions: time and space; and two key elements: nodes and arcs. Each node represents a location (airport) and a time t along the day, while an arc connects two nodes. Two types of arcs were considered: flight arcs and ground arcs. A flight arc represents a flight from one location to another for a certain time period. A ground arc represents the choice of remaining at the same airport for a certain time period. This is visualized in Figure 5, where the solid arrow represents a ground arc and the dashed lines represent flight arcs.

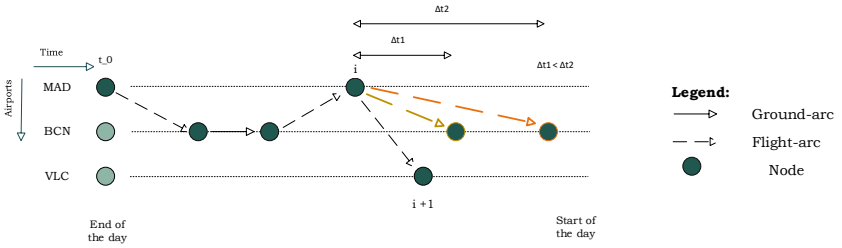

Fig. 5 Representation of a time-space network

The minimum time step between two nodes connected by a ground arc is set to 12 minutes, while the time step between two nodes connected by a flight arc is modeled depending on the duration of the flight. This approach, has potential to demonstrate the effect of cruise speed on network performance. This is illustrated with the yellow and orange arrows in Figure 5. Both flight arcs have the same origin and destination, but the orange is flown at a lower velocity than the yellow. Thus, the former must depart earlier to arrive at the same time as the latter. The outcome of the **Schedule Path Explorer** is a time-space network graph spanning all possible flight sequences in a day for a certain aircraft.

Best Pathfinder
Whenever an arc is considered, a weight (W_l) is computed and associated with it. This weight is then used by the **Best Pathfinder** subroutine to determine the sequence of flights which maximizes the objective function expressed in Equation 19. This sequence of flights also has to comply with the set of constraints detailed in Equation 20-Equation 25. The Bellman-Ford shortest path algorithm is used to achieve the desired result [24]. After finding the best sequence of flights for one day, the algorithm moves to the next step (previous day) and repeats both the **Schedule Path Explorer** and **Best Pathfinder** subroutines until the beginning of the week is reached. Note that airport continuity was ensured from one day to the next.

Objective Function
A multi-objective function is considered in which both profit and CO_2 emissions are taken into account. To establish a fair comparison between the two objectives, the CO_2 emissions were monetized by making use of a cost per emission C_e [€/ton]. The relative importance of the two separate objectives is controlled with the parameters w_p and w_e, where the former is the relative importance of profit and the latter is that of CO_2 emissions, with their sum equal to 1. Details on how profit p_l was estimated can be found in Section II.C.5 and details on how the CO_2 emissions (e_l) were estimated can be found in subsection II.B. Table 2 gives the definitions for all the sets used in the model, including set **P**.

$$\max \mathcal{J} = \sum_{l=1}^{\mathbf{P}_p} W_l = \sum_{l=1}^{\mathbf{P}_p} w_p \cdot p_l - w_e \cdot e_l \cdot C_e \qquad \forall p \in \mathbf{P} \tag{19}$$

Table 2 Model sets

Set	Description
P	All feasible flight schedules
$\mathbf{P}_p$	Sequence p of feasible flights in P, where p = [1,2,3,...]
A	All aircraft types in the database
N	All airports in the network
T	All timesteps in a day of operations

Constraints
A feasible flight schedule is one for which all flight legs l comply with a number of constraints. *Runway Constraints* (Equation 20 and Equation 21) ensure that the runway length (L_i, L_j) is long enough for a certain aircraft **a** to both take-off and land at airports i and j, respectively. Additionally, the total number of passengers transported from airport i to airport j is limited by either the demand at time t or by the capacity of the aircraft (Equation 22). Note that a maximum load factor LF is taken into account to model the spoilage of passengers which often occurs in airline operations [25]. *Range Constraints* Equation 23 ensure that the range of an aircraft **a** carrying a certain payload m_{pay} (which must comply with the *Capacity Constraint*) is sufficient to travel the distance between airports i and j in feasible flight leg l. Two additional constraints, *Transfer Passengers Constraint* (Equation 24) and *Utilization Constraint* (Equation 25) ensure that for all flight schedules in **P** no transfer passengers are left at the hub ($w_{l,hub}$) at the end of the day and that for all flight schedules in **P**, the sum of the flight block time (bt) of all flights in a certain flight schedule p is smaller than or equal to the maximum allowable aircraft utilization ($UT_{\max}$).

Take-off Runway Length Constraint: $$L_i \leq \text{TOL}_a \quad \forall i \in \mathbf{N} \quad , \forall a \in \mathbf{A} \tag{20}$$

Landing Runway Length Constraint: $$L_j \leq \text{LD}_a \quad \forall j \in \mathbf{N} \quad , \forall a \in \mathbf{A} \tag{21}$$

Capacity Constraint: $$u^t_{ij} + w^t_{ij} = \mathbf{min}(\text{CDdemand}^t_{ij}, \text{seats}_a \cdot \text{LF}) \quad \forall i, j \in \mathbf{N}, \quad \forall t \in \mathbf{T}, \quad \forall a \in \mathbf{A} \tag{22}$$

Range Constraint: $$R_a(m_{\text{pay}}) \geq \text{dist}_{ij} \quad \forall i, j \in \mathbf{N} \quad , \forall a \in \mathbf{A} \tag{23}$$

Transfer Passengers Constraint:
$$\sum_{l=1}^{\mathbf{P}_p} w_{l,\text{hub}} = 0 \quad \forall p \in \mathbf{P} \tag{24}$$

Utilization Constraint:
$$\sum_{l=1}^{\mathbf{P}_p} \text{bt}_l \leq \text{UT}_{\max} \quad \forall p \in \mathbf{P}, \quad \forall a \in \mathbf{A} \tag{25}$$

3. Fleet Selection & Airline Schedule

At each iteration, the selection of a new aircraft was made in accordance with the objective function defined by Equation 26. Note that $c_{ownership,a}$ is the cost of owning aircraft **a** from the set of aircraft **A**.

$$\max \mathcal{H} = \mathcal{J} - w_p \cdot c_{\text{ownership},a} \quad a \in \mathbf{A} \tag{26}$$

4. Demand Modeling

Demand modeling follows the method by *Wang* [26] to determine the number of passengers transported on each flight.

Unconstrained Demand

Unconstrained demand is the estimated weekly number of passengers desiring to fly from airport *i* to airport *j*. This data was attained through an itinerary and passenger flow analysis based on actual flight data. [h] People's willingness to fly in reality fluctuates throughout the day and week, however, here it is assumed to be distributed evenly over a week.

Passenger Demand Distribution

To distribute the daily unconstrained demand (UDemand) across the day, a demand probability function was used ($p(t)$). This reflects people's willingness to fly at specific times, modeled as a normal distribution with a mean corresponding to the midpoint of the operational day and a standard deviation of three hours. In reality, two demand spikes during a single day—in the early morning and late afternoon [13, 27, 28]—can be expected to reflect common passengers' departure time preferences. While the proposed method can flexibly accommodate any temporal redistribution pattern, the current approximation was deemed sufficient for testing and validating the proposed approach in our case study. In order to construct the *Passenger demand distribution* function (F_t), operational hours were split into blocks of 12 min and the probability density function value at each time step t was multiplied by the unconstrained demand (Equation 27). A visual representation is shown in Figure 6 for an arbitrary OD-pair. Because it is simplistically assumed demand does not vary throughout the week, the demand distribution function is repeated for each day of the week. This demand distribution function must be created for each OD-pair in the network.

$$F_t = p(t) \cdot \text{UDemand} \tag{27}$$

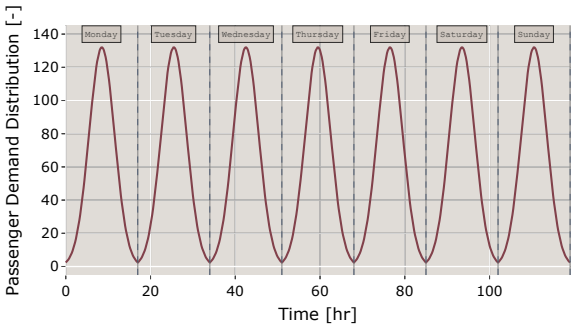

Fig. 6 Passenger Demand Function

Constrained Demand

Constrained demand is bound not only by passengers' itinerary but also by aircraft capacity. To estimate the total demand between airport *i* and airport *j* at time *t* it is assumed that all demand comprised within 1 hour of departure time (i.e. the attraction band) wishes to board the flight. A distinction is made between transfer and direct demand. A typical transfer is composed of two legs: **spoke-hub** and **hub-spoke**. Since the schedule is created starting at the end of the day, for every transfer itinerary, the second leg is considered first (**hub-to-spoke**). Hence, to determine the transfer

[h] OAG Aviation Data - `www.oag.com`

demand of a **hub-to-spoke** flight, the total unconstrained transfer demand wishing to travel from any other spoke in the network to the current spoke must be computed. Now, a *Transfer Passenger Demand Distribution* function can be created (Equation 27) and the constrained transfer demand can be computed according to Equation 28.

For a **spoke-hub** OD-pair, the constrained transfer demand is calculated differently. For this type of OD-pair, special attention is given to the transfer passengers for which a **hub-spoke** leg has been considered already. These passengers are given priority over direct passengers in the flight and thus automatically allocated, to minimize the number of schedule paths for which transfer passengers are left at the hub at the end of the day. Constrained direct demand follows Equation 28, however, F_t is created directly from the unconstrained direct demand between the considered OD-pair.

$$\text{CDemand} = \int_{t-1}^{t+1} F_t \quad dt \tag{28}$$

Served Demand

Once a flight is added to the schedule, transported passengers should be removed from the demand. The method used by *Wang* [26] was used to achieve this. This method considers that demand closer to the departure time is more likely to be captured than the demand slightly further. Hence, starting at departure time t, the *Passenger Demand Distribution* of the OD-pair being considered is set to zero. This is propagated out in both directions (towards earlier in the day and towards later in the day), until the integral under the *Passenger Demand Distribution* is equal to the number of passengers transported. This model was adopted, instead of *Rubbrecht's* [29], because it avoids the simultaneous scheduling of flights for the same OD-pair, which is deemed unrealistic from an airline perspective. Figure 7 displays an example of the *Passenger Demand Distribution*, after served demand has been removed.

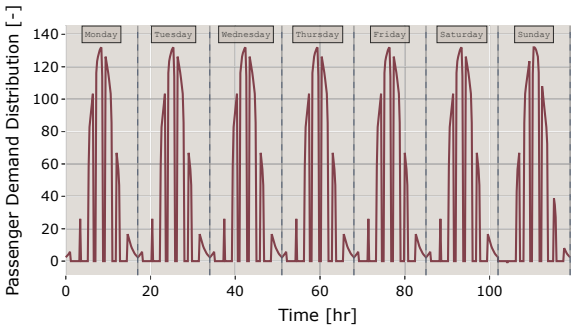

Fig. 7 Passenger Demand Function once served demand has been removed

5. Profit Estimation

The profit of flying a certain flight is dependent solely on the revenue and the cost of operating such a flight. The former translates into Equation 29, which demonstrates the total profit p attained in a feasible flight sequence $\mathbf{P}_p$, where r_l and c_l are the revenue and the operating cost of feasible flight leg l.

$$p = \sum_{l=1}^{\mathbf{P}_p} (r_l - c_l) \quad \forall p \in \mathbf{P} \tag{29}$$

Revenue

Revenue depends on the amount of passengers that are being transported and on the fare. All seats are charged the same fare. Furthermore, no distinction is made between transfer passengers and direct passengers. Thus, for each flight leg, revenue is expressed with Equation 30. Note that since revenue does not change with flight distance, the model has a preference for choosing shorter flights as these are cheaper to operate.

$$r_l = \text{fare} \cdot (u_l + w_l) \tag{30}$$

Operating Cost

Operating cost include not only *crew costs*, *airport costs* and *navigation fees* but also *fuel costs*, *electricity production costs* and aircraft *ownership cost*. Crew costs were estimated based on the method given by *Roskam* [30]. Crew is

assumed to be composed of a captain, first officer and cabin crew members, with regulations requiring one cabin crew member for every 50 seats. Crew costs are estimated based on an assumed annual salary[i,j], an annual amount of flight hours and the flight's block velocity.

Airport costs are estimated following the method proposed by *Wang* [26], which considers two separate types of airport sub-costs: the ground-handling & parking fees and the landing fees; airport-specific taxes are not taken into account. Furthermore, the key parameters driving these costs on a specific flight are the aircraft's maximum take-off weight (MTOW) and the number of seats in the aircraft. Note that, to emulate the loss of profit from choosing a ground arc at time step t instead of a flight arc, it is considered that the cost is equal solely to the ground-handling fees.

Navigation fees were also estimated with the method detailed by *Wang* [26], and were made dependent on the aircraft's MTOW and the flight's distance. Moreover, the costs associated with purchasing fuel and purchasing electricity are modeled by assuming a fuel and electricity price and by taking into account the fuel and battery energy consumed during the flight which is being considered.

Ownership costs differentiate between conventional aircraft and hybrid-electric aircraft, with the latter likely to be more expensive due to the battery. Ownership costs of a hybrid-electric aircraft are assumed to be 20 % higher than the cost of owning their conventional counterpart. Based on the purchasing price of each selected aircraft, the weekly ownership cost is computed with the relationship given by *Jansen & Perez* [31].

D. Coupling Strategy

The objective behind devising a coupling strategy lies in the idea of using the information attained with the *Fleet & Scheduling Module* and deducting trends and modifications to the aircraft which could potentially benefit the network.

1. Coupling Variables

The two aircraft design variables which were identified to have the largest influence on the performance of the network were the aircraft's design range and the aircraft's design payload. The former directly correlates with route flexibility and servicing, while the latter correlates with the amount of demand that can be captured. Additionally, aircraft capacity is related to the amount of profit a given airline makes at any given time, while the selection of the design range affects the fuel consumed. Moreover, this becomes increasingly more relevant when considering hybrid-electric aircraft, as with the addition of the battery, the design range plays a crucial role in the weight penalty the final design suffers [5].

2. Clustering Method

Flights for each of the aircraft selected during the *Fleet & Scheduling Module* were clustered in terms of passengers carried and distance flown. This provides insight into what types of routes are flown and whether or not it makes sense to redesign the aircraft.

To cluster flights in terms of payload and range, the *Kmeans clustering method*[k] was used. This is an unsupervised machine learning algorithm which clusters data into a specified number of clusters by minimizing the sum of squares within each cluster. This implies dividing a set of **M** samples **X** into **K** separate clusters, for which each is associated with a mean value μ_j. These mean cluster values were used to determine whether modifications to the aircraft design were desirable.

Additionally, to determine the best number of clusters to fit the data, the "Kneedle Algorithm" developed by *Satopaa et al.* [32] was used. The algorithm was created to detect the point at which the cost of increasing some parameter in a system is no longer worth the improvement in the system's performance. It can be used in situations where for opposing variables, for which a trade-off is required, a sensible design point must be selected.

In the current application, it is used to select the number of clusters by determining where an increase in the number does not result in a substantial improvement to the fit of the "centroids" to the data. This is visualized in Figure 8, for which the distortion score represents how well the cluster centroids fit the data, and k represents the number of clusters. For this specific example, three clusters are the most sensible choice and as illustrated in Figure 9.

[i] `https://www.salaryexpert.com/salary/job/flight-attendant/spain` [Accessed: 22/12/2023]

[j] `https://worldaviationato.com/en/airplane-pilots-salary/` [Accessed: 22/12/2023]

[k] `https://scikit-learn.org/stable/modules/clustering.html` [Accessed: 15/12/2023]

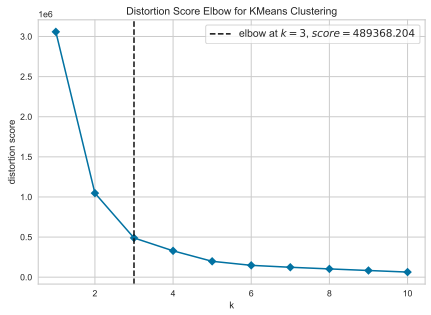

Fig. 8 Cluster number versus distortion score for example data

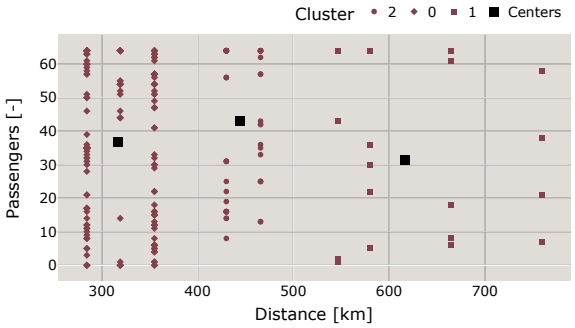

Fig. 9 Example of clusters in terms of passengers and distance flown

III. Case Study Description & Framework Verification

This section elaborates on the case study used to verify the framework. This case study was used to construct a reference scenario, which was used to verify the *Fleet Assignment and Scheduling Module* by focusing on whether the module is able to correctly represent the decision making process of an airline. Additionally, the reference scenario is used for the later analysis in Section IV, where hybrid-electric aircraft are added to the network. The hybrid-electric design method has already been partially verified by *Scheers*, *Hoogreef* and *de Vries* [10][33][3].

A. Case Study Description

A regional airline case study was selected, considering this as the target market for hybrid-electric aircraft.

1. Airline Characteristics

The case study is based on the Spanish airline Air Nostrum as it is a regional airline with routes suited for the potential application of hybrid-electric aircraft, and because an unconstrained demand estimate between the OD-pairs in the network was available from OAG data.[h]. The airline's network is composed of 40 airports and a total of 109 routes operated by three types of aircraft: the ATR 72-600, the Bombardier CRJ200 and the Bombardier CRJ1000. The characteristics of these aircraft were used as a baseline for their hybrid-electric counterparts.

A subset of the network was used to reduce computational time. Selected airports and routes were required to represent the entire network as much as possible, implying that they should not only represent variation in demand and range, but also allow transfer passengers. Furthermore, it was considered imperative that the subnetwork would include routes with the following demand-distance combinations: *low demand - short range*, *high demand - short range*, *low demand - long range*. Note that the combination *high demand - long range* is not considered since the Air Nostrum network does not encompass this type of route. The longest route is 1186 km while the shortest is 209 km. Therefore, the off-design study for every aircraft (both conventional and hybrid) was restricted to a range between 100 km and 1300 km. Given the aforementioned considerations, 13 airports were selected. The information regarding the airports' geographical location was retrieved from *Openflights*[l], while the runway length was retrieved from *AirportDB*[m]

2. Aircraft Characteristics

Table 3 summarizes the aircraft characteristics which were considered to prescribe the top-level requirements. These were used as baseline values for the reference conventional aircraft and reference scenario, and as top-level requirements for the hybrid counterparts. Considering the scope of the project, although the *Bombardier CRJ200* and *Bombardier CRJ1000* are initially turbofans, the baselines were converted into turboprops. Due to the need to limit propeller tip speeds and to avoid loss of efficiency at very high altitudes, both the cruise speed and the cruise altitude were reduced. The cruise altitude and the cruise velocity of the *ATR 72-600* were used as a reference. Moreover, the approach speed

[l] `https://openflights.org/` [Accessed: 18/11/2023]
[m] `https://airportdb.io/#findairport` [Accessed: 18/11/2023]

(V_{app}) was reduced for both *Bombardier* aircraft. The real approach speed for the *Bombardier CRJ1000* is 65[n] m/s and for the *Bombardier CRJ200* is 69 [o] m/s. The former design modifications have of course implications in the network performance. Due to the difference in cruise velocity, it would be unrealistic to assume it would be possible to serve all the original routes. However, this is not considered to be an issue as the analysis is centered around comparing different case studies, rather than providing absolute results.

Table 3 Top-level aircraft requirements

Parameter	Aircraft		
	ATR72-600	*CRJ200-prop*	*CRJ1000-prop*
Seats [-]	72 [p]	50[q]	100[r]
R_{design} [km]	1370 [p]	3148[q]	3056[s]
h_{cruise} [m]	7620[t]	8000[a]	8000[a]
V_{cruise} [m/s]	142[p]	140[a]	140[a]
V_{app} [m/s]	58[u]	60[a]	60[a]
AR [-]	12[p]	9.3[q]	8.9[r]
n [-]	2[p]	2[q]	2[r]
TOL [m]	1315[p]	1920[q]	2030 [n]
Cost [million €]	24[v]	22.3[q]	23.1[n]

[a] Values adjusted to transform aircraft into turboprop aircraft.

B. Verification

The *Air Nostrum* case study was used as a reference to verify the correct working of the framework. A reference scenario was not only constructed to serve as basis of comparison for all the scenarios evaluated in Section IV but also to verify the correct working of the *Fleet Assignment and Scheduling Module*. Air Nostrum demand data and conventional aircraft along with the airport data were fed as inputs to the *Fleet Assignment and Scheduling Module*. Both objectives (profit and emissions) were considered to be equally important.

In this scenario, the *CRJ200-prop* aircraft was not selected since it is the smallest of the options and the analysis was performed on a subset of the network, which excluded routes with extremely small demand. The reference fleet is composed of 4 *ATR72-600* and 7 *CRJ1000-prop* aircraft; results are summarized in Table 4. Several network key performance indicators (KPIs) are used: total profit, total cost, percentage of demand served, number of OD-pairs served, cost available seat kilometer (CASK), revenue available seat kilometer (RASK) and total CO_2 and NO_x emissions.

It is important to note that the longest route included in the schedule was 664km, meaning all longer routes were not considered profitable. Longer routes imply fewer flights can be allocated in one day and since the fare price does not vary with the length of the mission, longer missions end up producing less profit. They generate revenue equivalent to shorter routes but consume more fuel and reduce the number of possible flights in one day.

Table 4 Key Performance Indicators of the Reference Scenario

Variable	**Profit** [€]	**Cost** [€]	**Demand Served** [%]	**OD-pairs Served** [-]	**CASK** [€/km]	**RASK** [€/km]	**CO_2** [kg]	**NO_x** [kg]
Value	$2 \cdot 10^6$	$1.4 \cdot 10^6$	33	8	$3.9 \cdot 10^{-2}$	$1.25 \cdot 10^{-1}$	$1.4 \cdot 10^6$	$1.8 \cdot 10^3$

[n] https://aerocorner.com/aircraft/bombardier-crj-1000/ [Accessed: 20/09/2023]
[o] https://skybrary.aero/aircraft/crj2 [Accessed: 20/09/2023]
[p] https://www.atr-aircraft.com/ [Accessed: 20/09/2023]
[q] https://www.flyradius.com/bombardier-crj200/specifications [Accessed: 20/09/2023]
[r] https://www.flyradius.com/bombardier-crj1000/specifications [Accessed: 20/09/2023]
[s] https://pdf.aeroexpo.online/pdf/bombardier/crj-series-brochure/169445-101.html [Accessed: 20/09/2023]
[t] https://www.caribbean-airlines.com/#/our-fleet/atr-72-600
[u] https://skybrary.aero/aircraft/at76 [Accessed: 20/09/2023]
[v] https://aerocorner.com/aircraft/atr-72-600/ [Accessed: 20/09/2023]

IV. Results & Discussion

The Air Nostrum case study was used as a test case to understand how off-design performance of hybrid-electric aircraft influences the performance of a regional airline network. In particular to understand what are the key variables in the trade-off between conventional or hybrid-electric aircraft and how hybrid-electric aircraft could be better tailored to a regional airline network.

A. Hybrid-Electric Design Exploration

The following section analyses off-design performance of HE aircraft design changes for different design ranges and power splits. Furthermore, the effect of off-design cruise Mach numbers is also studied.

1. Baseline Hybrid-Electric Designs

Initially, all 3 hybrid-electric aircraft were sized with 5% supplied power split in all nominal flight phases. However, for the *CRJ200HE* this led to a battery which did not fit inside the aircraft. A similar issue occurred for the *CRJ1000HE*. Although there was space to store the battery, the span of the aircraft surpassed the 36m span constraint. Therefore, the baseline hybrid-electric design of these aircraft use 4% a supplied power split.

Furthermore, it was observed that even when setting the design power split to a value as little as 5% there was a significant increase in MTOM. Table 5 summarizes the main results and provides the Δ in terms of percentage with respect to the correspondent conventional counterpart. It was observed that the larger the design range, the larger the increase in MTOM and consequently the larger the increase in wing span (percentage wise). Moreover, one can also notice the large increase in fuel consumption for the *CRJ200HE* and *CRJ1000HE* due to the increase in MTOM and drag penalty due to the low aspect ratio of these aircraft.

Table 5 Initial Hybrid-Electric Aircraft design, battery energy density = 350 Wh/kg

Aircraft	**Power split** [%]	$\mathbf{R}_{\text{design}}$ [km]	$\mathbf{M}_{\mathbf{bat}}$ [kg]	**MTOM** [kg]		**b** [m]		M_f [kg]	
				Value	Δ [%]	*Value*	Δ [%]	*Value*	Δ [%]
ATR72-600HE	5	1370	3.31	30.8	+25	32	+11.8	2.09	+3.7
CRJ200HE	4	3.15	5.97	31.2	+66	27	+26.8	4.13	+38.4
CRJ1000HE	4	3.06	10.5	57.5	+64.5	36	+26.8	7.26	+39.4

2. Off-Design Performance

The off-design analysis for the three baseline HE aircraft is presented in Figure 10. Within the considered range of mission lengths (100-1300 km), Figure 10 provides information on three important variables for each of the hybrid-electric aircraft. ΔM_{fuel} is the percentage difference in terms of fuel consumed for given a certain payload-range combination, $\phi*_{\text{cruise}}$ is the maximum attainable cruise power split and $\eta_{p,\text{climb}}$ is the propulsive efficiency during climb (here propulsive efficiency refers to the ratio between $T \cdot V_0$ and the increase in kinetic energy of the air). The results for different payload masses can be identified by the color/dash type of the lines.

It can be observed that baseline HE aircraft fuel consumption gradually reduces with mission length, event below its conventional equivalent. However, there is also a non-linear relationship between $\phi*_{\text{cruise}}$ and the length of the mission. For very short mission lengths, below 300km, in spite of the maximum attainable cruise power split reaching values as high as 80%, the fuel consumption of the baseline HE aircraft begins to worsen, and can even become worse than its conventional counterpart. Several factors have been identified that influence this behavior. On one hand, the maximum attainable supplied power split during cruise is limited by the operational envelope of the gas turbine. This limit to the power split is found to be roughly equal to 85% for all baseline HE aircraft and irrespective of the payload mass.

The consequence of the aforementioned behavior is that for very small missions, the battery capacity is not fully used. However, this is not sufficient to explain why for very small missions the HE aircraft seem to suffer in terms of performance. Ultimately, this is attributed to the fact that HE aircraft suffer from a lower propulsive efficiency during climb and thus require a more fuel to achieve the same thrust. This is true for all aircraft and irrespective of the mission length as can be seen from Figure 10. As the mission length decreases, the climb segment becomes increasingly more dominant in terms of the total fuel consumed. Therefore, once the upper bound for maximum attainable cruise power split is reached, as the mission length continues to decrease, the HE aircraft fuel savings during cruise are not sufficient

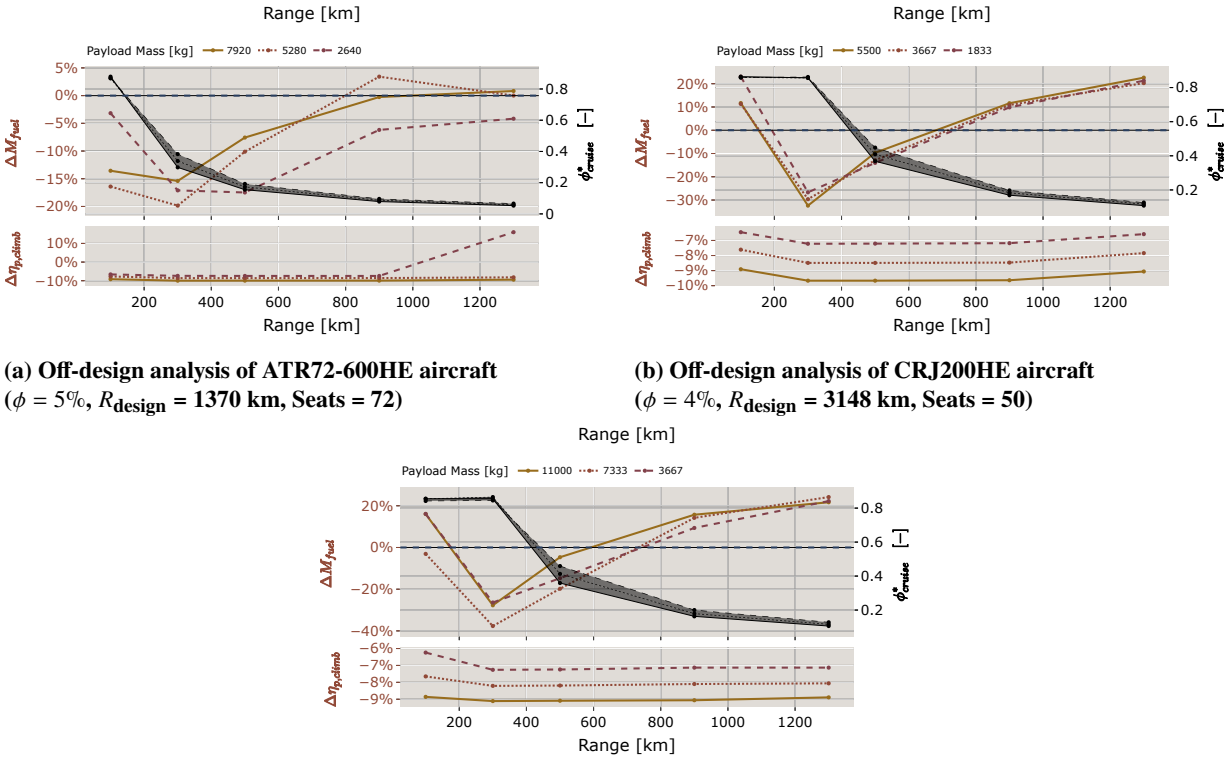

(a) Off-design analysis of ATR72-600HE aircraft
(ϕ = 5%, R_{design} = 1370 km, Seats = 72)

(b) Off-design analysis of CRJ200HE aircraft
(ϕ = 4%, R_{design} = 3148 km, Seats = 50)

(c) Off-design analysis of CRJ1000HE aircraft
(ϕ = 4%, R_{design} = 3056 km, Seats = 100)

Fig. 10 Difference in fuel consumption of hybrid-electric aircraft with respect to conventional counterparts

to compensate for the larger fuel consumption during climb. This highlights the importance of the hybrid powertrain control variables in the minimization of their fuel consumption.

Additionally, it appears that for all three HE aircraft, there are similar "switching points". Around 300km, the fuel consumed by these aircraft shifts from progressively decreasing to progressively increasing. Nevertheless, it is important to note the discrete and coarse nature of the analysis, does not allow to identify for each aircraft when exactly the largest fuel consumed reduction is achieved.

Finally, for smaller design ranges (*ATR72-600E*), it is possible to observe fuel savings already at mission lengths close to the design range, while for larger design ranges, fuel savings are restricted to mission lengths up until roughly 23% of the design range. Inspecting Table 5 for the fuel used along with the weight penalty, it becomes evident how aircraft sized for a shorter design range save fuel for a greater area of the domain. Moreover, the small aspect ratio of the *CRJ* aircraft plays an important role here and shifts the curves to higher fuel consumption values.

3. Cruise Mach Number Variation

The effect of modifying the cruise Mach number on the off-design performance of HE aircraft was evaluated for the baseline *ATR72-600HE* and a redesigned *CRJ1000HE-s*. The redesign has a shorter design range of 1370km and a design power split of 5%. Figure 11 displays how modification of the cruise velocity affects the fuel consumed for different payload-range combinations. It must be noted that all HE aircraft fuel profiles (both on and off-design) were compared with the fuel profile of their conventional counterpart flying at design cruise speed.

Cruising at a higher velocity yields a higher fuel consumption since accelerating to a higher velocity requires more fuel to be consumed during climb and acceleration, and cruising at a higher velocity implies a higher power and thus higher fuel consumption. When cruising at a lower velocity the opposite reasoning is applied. However, this is only true when we remain in an acceptable operating envelope of a particular aircraft design, as illustrated in the idealized performance diagram in Figure 12.

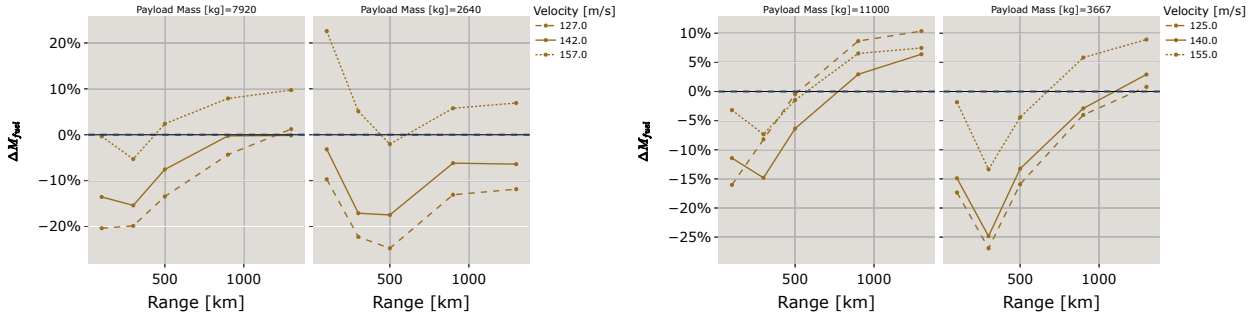

(a) Off-design analysis of ATR72-600HE aircraft (ϕ = 5%, R_{design} = 1370 km, Seats = 72)

(b) Off-design analysis of CRJ1000HE-s aircraft (ϕ = 5%, R_{design} = 1370 km, Seats = 100)

Fig. 11 Variation with cruise velocity of off-design analysis for hybrid-electric aircraft

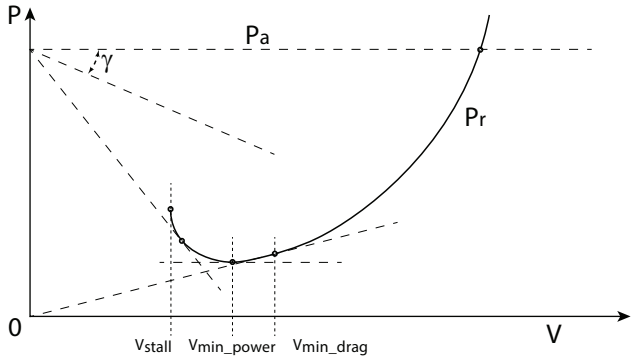

Fig. 12 Impression of idealized performance for a propeller aircraft in steady symmetric flight, inspired by [34]

This is demonstrated by the *CRJ1000HE-s* in Figure 11b. When cruising at a lower velocity, more fuel is consumed. This is caused by top-level requirements set for this aircraft, in particular the combination of approach speed and aspect ratio. At even lower cruise speeds, the aircraft starts approaching stall speed and power required for steady symmetric flight quickly increases. When flying at a lower capacity the aircraft, this sensitivity changes as at lower speed the aircraft in steady symmetric flight is further away from $C_{L_{\max}}$ and thus further away from the stall speed.

4. Design Point Variation

Design Power Split Ratio

In order to analyze the effect of modifying the design power split on the off-design performance of hybrid-electric aircraft, the design power split ratio of the aircraft *CRJ1000HE-s* and *ATR72-600HE* was modified. Both the aircraft are sized for the same design range and the same design power split ratio (equal to 5% or 10%). Nevertheless, they have different design payloads. Table 14 in Appendix B provides further details on the performance and characteristics of these aircraft designs at their design point.

In Figure 13 and Figure 14, ΔM_{fuel} represents, the difference in total fuel consumption at a certain payload-range combination, between the hybrid-electric aircraft and their conventional counterpart. Thus, for the case of the *CRJ1000* it is important to consider the difference in design range between the HE aircraft and its conventional counterpart. Sizing for a smaller design range results in larger fuel savings for a larger portion of the domain considered, as demonstrated in Section IV.A.1. Therefore, it does not affect the analysis on the effect of modifying design power split.

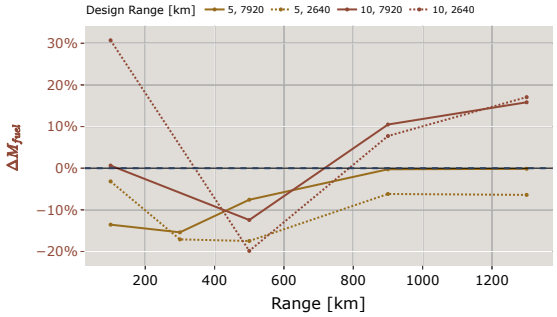

Fig. 13 Off-design analysis of ATR72-600HE (ϕ = 5%, R_{design} =1370 km, Seats = 72)

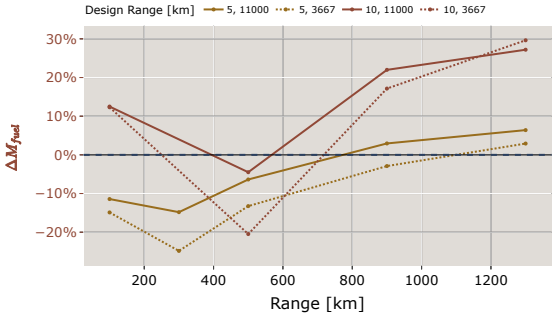

Fig. 14 Off-design analysis of CRJ1000HE (ϕ = 5%, R_{design} =1370 km, Seats = 100)

When inspecting Figure 13 and Figure 14 one can observe that as the mission length decreases the aircraft sized for a power split of 10% experiences a much steeper decline in fuel consumption. Furthermore, when looking at larger mission lengths, the former consumes relatively more fuel than aircraft with lower design power split. Similar to sizing a HE aircraft for a larger range, when sizing it for a larger power split, the weight penalty due to the increase in battery weight can restrict fuel saving potential to a smaller portion of the domain.

Design Range

To analyze the effect of design range on the off-design for HE electric aircraft, four different design ranges were considered. The *CRJ1000-HE* aircraft were redesigned for 1370, 620, 450 and 300km design range and a design power split of 5%. Note that these design ranges are not chosen arbitrarily, these were selected by making use of the coupling strategy explained in Section II.D. This procedure shall be further elaborated upon in Section IV.B. Now, the focus is on evaluation of the off-design performance. Table 14 in Appendix B details the on-design performance and characteristics of the aforementioned *CRJ1000-HE* redesigns.

Figure 15 displays for each redesign the change in fuel consumption per payload carried, at different payload-range combinations, with respect to the conventional counterpart. Unlike previous analysis, the metric of comparison is the change in fuel per payload carried since this is fairer as some of the comparisons need to be made beyond the harmonic point in the payload-range diagram.

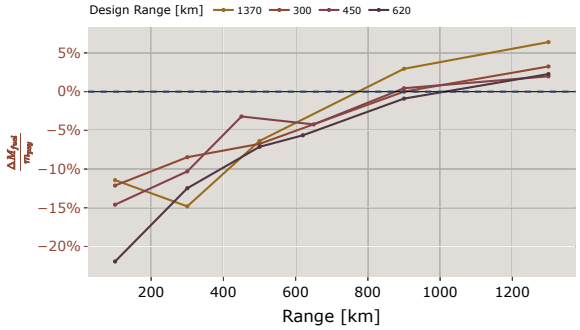

Fig. 15 Off-design comparison of CRJ1000HE for several R_{design} (ϕ = 5%, Seats = 100)

Inspecting Figure 15, one can note that the trends of fuel savings per payload carried are similar across the aircraft sized for design ranges of 300, 450 and 620km, especially for large mission lengths. However, as has already been partially observed in Section IV.A.1, it appears that aircraft designed for larger ranges experience a stronger decline in terms of fuel consumed as the mission length becomes increasingly smaller. This is then reflected by the fact that at very short ranges (below 300km) the largest fuel savings are attained by the aircraft with a design range equal to 620km. Unlike the aircraft sized for 1370km, there's no kink in the decreasing fuel consumption for decreasing mission lengths until 100km. This indicates that for these aircraft the upper bound for the $\phi{*}_{cruise}$ has not been reached. Ultimately, the observations indicate that reducing the design range, up to a certain threshold, yields fuel saving potential for off-design missions. This threshold is likely dominated by the climb performance of the aircraft.

B. Fleet Assignment and Scheduling Analysis

The following section presents the impact of different design power splits and design ranges on airline network performance. Section IV.A elaborated on the off-design performance of these designs, however, the way in which these redesigns were selected was not discussed. From these redesigns, several scenarios were constructed which are analyzed in Sections IV.B.1 and IV.B.3. Finally, Section IV.B.2 elaborates on how cruising at off-design conditions impacts the network performance.

1. Fully Hybrid-Electric Fleet

The baseline HE aircraft analyzed in Section IV.A.1 were placed in the network along with their conventional counterparts (defining scenario **A** in Table 6). No hybrid-electric aircraft were selected and thus the final selected fleet was exactly the same as in the reference scenario (refer to Section III.B and Table 7). A similar result was observed in earlier studies [33] and is associated with the ownership cost being 20% higher than the conventional counterpart.

Since the unnecessarily large design range of the *CRJ-HE* aircraft does not serve the (subset) of the network, the *CRJ1000HE* was resized for a design range of 1370km. Once this aircraft was added, the fleet assignment and schedule creation, one HE aircraft was selected. Based on the clustering of ranges flown in Figure 9, several redesigns were made as presented in the previous Section and Appendix B.

Table 6 Scenario setup for A, B, C, D and J[w].

Scenario	Initial Fleet	Objective Function Weights $[w_p, w_e]$	Velocity
A	CRJ1000-KE; CRJ200-KE; ATR72-600-KE; CRJ1000-HE-3056-4; CRJ200-HE-3148-4; ATR72-600-HE-1370-5	[0.5,0.5]	Constant
B	CRJ1000-HE-1370-5, CRJ200-HE-1370-5, ATR72-600-HE-1370-5	[0.5,0.5]	Constant
C	CRJ1000-HE-1370-5, CRJ1000-HE-620-5, CRJ1000-HE-450-5, CRJ1000-HE-300-5	[0.5,0.5]	Constant
D	CRJ1000-HE-1370-10, ATR72-600-HE-1370-10	[0.5,0.5]	Constant
J	CRJ1000-HE-1370-5, CRJ200-HE-1370-5, ATR72-600-HE-1370-5	[0.5,0.5]	Variable

Table 6 summarizes the main characteristics of the different scenarios analyzed in the following section, for all Scenarios (except **A**) only hybrid-electric aircraft are available for fleet assignment and scheduling. Comparing **B** to **C** allows for analyzing the effect of design range on the network's performance. Comparing **B** to allows for understanding the effect of design power split. Finally, **J** allows studying the effect of cruising at off-design Mach numbers. The different scenarios considered were evaluated according to several key performance indicators and compared to the reference scenario described in subsection III.B, which would also be the result of **A**. Figure 16 illustrates this comparison (for the fleet in Table 7). Any point outside the black circular line indicates a larger KPI value and vice-versa.

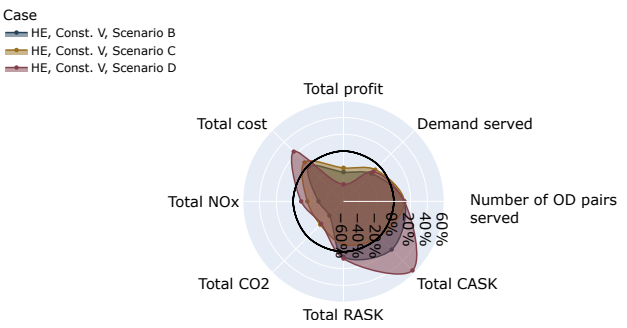

Fig. 16 KPI comparison between scenarios B, C and D, circle indicates reference scenario (and output of A)

Table 7 Fleet composition for hybrid-electric scenarios A, B, C, D and J

Scenario	Final Fleet
A	(**7**) CRJ1000-KE, (**4**)ATR72-600-KE
B	(**7**) CRJ1000-HE-1370-5, (**3**)ATR72-600-HE-1370-5
C	(**12**) CRJ1000-HE-300-5
D	(**5**) CRJ1000-HE-1370-10, (**6**)ATR72-600-HE-1370-10
J	(**3**) CRJ1000-HE-1370-5, (**6**)ATR72-600-HE-1370-5

[w]Note the naming convention for the different aircraft designs: Aircraft type- Powertrain type- R_{design} - ϕ_{design}; An example of an aircraft design according to this naming convention is: *Bombardier CRJ1000-HE-1370-5*

In general, all scenarios suffer a significant loss in total profit, whilst at the same time showing significant savings in CO_2 and NO_x emissions. When comparing scenario **C** with scenario **B**, the loss of profit of the former is smaller than the loss of profit on the latter (-20% versus -25%). However, total cost of scenario **C** exceed those of scenario **B** (+5.6% versus -1.3%). This can be attributed to two factors: (1) in scenario **C** the fleet is composed of two extra aircraft and thus ownership costs are larger. The smaller ownership cost of scenario **B** compensate for its larger CASK. Given the fact that in scenario **B** there is a larger reduction in terms of CO_2 and NO_x emissions (-36%), the increased CASK can only stem from larger electricity costs or larger airport and navigation costs (due to larger MTOM). (2) scenario **B** has a larger RASK than scenario **C**. This indicates that either scenario **B** has a larger load factor or that on average shorter routes are flown. Given the way in which revenue is modeled, it is reasonable that there is a preference for shorter routes. Scenario **C** seems to prefer smaller power splits, which seems to indicate that the modeled electricity cost are outweighing the fuel saving potential of higher power split.

When comparing scenario **B** with scenario **D**, the former yields a smaller loss in terms of profit than the latter (-25% versus -39.7%). Both scenarios have CASKs larger than in the reference scenario, this is specially accentuated for scenario **D** and can be attributed to both larger fuel costs (larger CO_2 emissions when compared to scenario **B**) and larger airport and navigation costs. The latter is inferred from the fact that as seen in Section IV.A.4, increasing the power split from 5% to 10% yields a large weight penalty. Furthermore, the larger total cost associated with scenario **D** are also a result of its final fleet being composed by one extra aircraft compared to scenario **B**.

2. Cruise Mach Number Effect

Table 6 also summarizes the main characteristics of scenario **J**. Scenarios **B** and **J** only differ by the fact that the cruise velocity on each flight is allowed to be selected by the fleet assignment and scheduling module for **J**. When inspecting Figure 17 and Table 7, one can note that when the cruise velocity is allowed to vary the final fleet includes a larger number of *ATR72-600-HE-1370-5*. As seen in subsubsection IV.A.3, both aircraft types yield larger fuel savings when flying slower, however, the *ATR72-600-HE-1370-5* to a larger extent. Furthermore, flying faster allows for a larger flight frequency, but more fuel is consumed. In scenario **J** the framework plays with this paradox and for each flight it chooses to fly slower (thus saving fuel), on another flight it chooses to fly faster (to include an extra flight). Nevertheless, the loss of profit is still larger than for scenario **B** due to a smaller accumulated revenue. Although the total number of flights in both scenarios is nearly the same (644 for scenario **J** and 642 for scenario **B**), due to the smaller capacity of the *ATR72-600-HE-1370-5* fewer passengers are transported which is reflected in a loss of demand served.

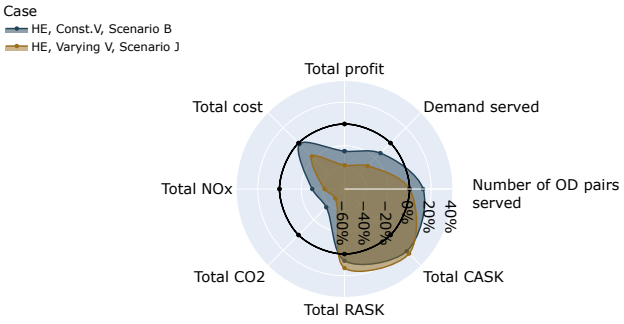

Fig. 17 Key performance indicators comparison between scenario B and J

3. Conventional and Hybrid-Electric Fleet

Table 8 summarizes the main characteristics of the scenarios analyzed for mixed fleets. These scenarios were constructed to understand how the performance of the network is affected if a mixed fleet is considered (both kerosene and hybrid-electric aircraft) and on the other hand how design range and design power split modify the former. Scenario **F** considered a mixed initial fleet, which includes the HE aircraft redesigns with a design power split ratio equal to 10%. When included in the Air Nostrum network, no HE aircraft was selected due to the same reasons as for scenario **A**.

Figure 18 displays the KPIs percentage difference between scenarios **E** and **G** and the reference scenario. When looking at scenario **E**, the final fleet composition (Table 9) differs from the reference scenario by only one aircraft: the *CRJ1000-HE-1370-5* was selected at the last iteration. From this modification, even though the *CRJ1000-HE-1370-5* aircraft has a larger ownership cost, total profit remains virtually the same (-0.01%). Although CO_2 emissions are reduced by 1.3%, scenario **G** yields a much larger reduction in CO_2 emissions (-15%). In scenario **G** a larger number of

Table 8 Characteristics of scenarios E, F and G. Green color refers to hybrid-electric aircraft

Scenario	Initial Fleet	Objective Function Weights $[w_p, w_e]$	Velocity
E	CRJ1000-KE, CRJ200-KE, ATR72-600-KE, CRJ1000-HE-1370-5, CRJ200-HE-1370-5, ATR72-600-HE-1370-5	[0.5,0.5]	Constant
F	CRJ1000-KE, ATR72-600-KE, CRJ1000-HE-1370-10, ATR72-600-HE-1370-10	[0.5,0.5]	Constant
G	CRJ1000-KE, ATR72-600-KE, CRJ1000-HE-1370-5, CRJ1000-HE-620-5, CRJ1000-HE-450-5, CRJ1000-HE-300-5	[0.5,0.5]	Constant

HE aircraft are selected. In spite of their larger ownership costs, with six *CRJ1000-HE-300-5*, total profit is reduced by only 1.35%. The increased ownership costs are mostly compensated by a reduction in operating cost. The latter stems from a reduction in fuel cost and airport cost (lower MTOM). This indicates that if ownership cost were to be the same between HE and KE aircraft, a mixed-fleet would yield larger profits. Nevertheless, further studies are required to confirm this. Moreover, the reduction in demand served, yet with an increase in RASK, indicates that shorter routes are flown. This seems reasonable, since, due to the small design range of the *CRJ1000-HE-300-5* aircraft, short routes (below 300 km) allow for the aircraft to fly at maximum capacity while yielding large fuel savings.

Combining KE and HE aircraft with a network-specific design range allows for initially capturing more demand (due to the reduced turnaround time of KE aircraft) at the expense of additional emissions. They are then compensated for by the HE aircraft flying short routes frequently and inexpensively. Furthermore, it is relevant to note the characteristics of the airline network being considered: many short routes with high demand. From both the off-design analysis conducted in Section IV.A and the observations made in this section it is clear how a network with these types of routes directly benefits from the introduction of HE aircraft.

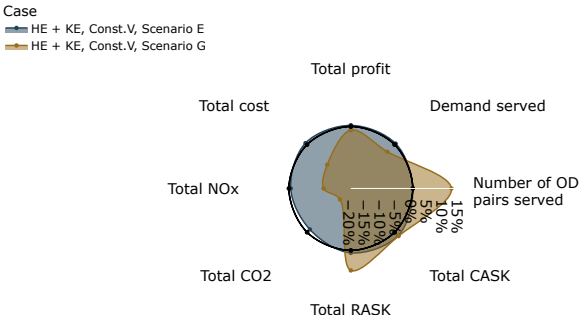

Fig. 18 Key performance indicators comparison between scenario E and G

Table 9 Fleet composition of mixed fleet scenarios

Scenario	Final Fleet
E	(**6**) CRJ1000-KE, (**4**) ATR72-600-KE, (**1**) CRJ1000-HE-1370-5
F	(**7**) CRJ1000-KE, (**4**) ATR72-600-KE
G	(**2**) CRJ1000-KE, (**2**) ATR72-60-KE, (**6**) CRJ1000-HE-300-5

C. Sensitivity Analysis

As described in subsection II.C, the fleet allocation follows a weighted objective function of profit and CO_2 emissions. Therefore, a sensitivity study was conducted to understand how the trade-off between these two objectives affects the performance of the network. Table 10 summarizes the characteristics of scenarios **H** and **I**, which were constructed based on scenario **G**, to assess different objective function weights. The results are presented in Figure 19 and Table 11.

Table 10 Characteristics of scenarios H and I. Green color refers to hybrid-electric aircraft

Scenario	Initial Fleet	Objective Function Weights $[w_p, w_e]$	Velocity
H	CRJ1000-KE, ATR72-600-KE, CRJ1000-HE-1370-5, CRJ1000-HE-620-5, CRJ1000-HE-450-5, CRJ1000-HE-300-5	[0.2,0.8]	Constant
I	CRJ1000-KE, ATR72-600-KE, CRJ1000-HE-1370-5, CRJ1000-HE-620-5, CRJ1000-HE-450-5, CRJ1000-HE-300-5	[1.0,0.0]	Constant

In general, attributing more importance to the profit-related objective (scenario **I**) leads to an increase in total profit (+26.5%) with a larger percentage of demand served (+29.5%). Evidently, this causes there to also be an increase in CO_2 (+26.6%) and NO_x emissions. A 1% increase in profit induces a 1% increase in CO_2 emissions. Interestingly, hybrid-electric aircraft are selected after the first fleet iterations. This is related to the effect discussed in Section IV.B.3, the trade-off between fast turnaround time of the kerosene aircraft and HE aircraft flying short routes frequently and inexpensively, which compensate some emissions. This also confirms the importance of turnaround time for fleet integration of (hybrid) electric aircraft, as shown in [4].

Counter-intuitively, giving more importance to emissions than profit (scenario **H**), reduces CO_2 emissions less than when equal importance is given to both objectives (-4.5% in scenario **H** and -15% in scenario **G**). However, it must be noted that in scenario **H** there is a growth in demand served (+9%) and the selected fleet generates a reduction in CO_2 emissions. Given the characteristics of the network that is studied (many short routes with high demand), the most profitable routes are also those that require least time and cost. As seen in Section IV.A, some short missions yield larger reductions in fuel consumption than others. Furthermore, both objectives are not entirely uncorrelated; reducing emissions also implies reducing fuel consumed and thus fuel costs. When prioritizing the emission objective the "greenest" routes within the short routes are selected which in turn not only yield lower emissions but also a higher profit. Consequently, during the iteration process, this effect accumulates and a larger number of aircraft are selected, serving more demand.

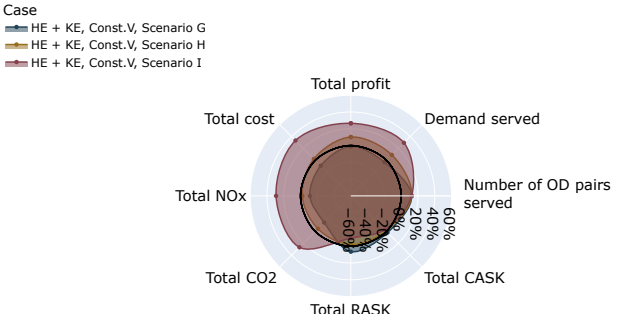

Fig. 19 Key performance indicators comparison between scenarios G, H and I

Table 11 Fleet composition of scenarios

Scenario	Final Fleet
G	(**2**) CRJ1000-KE, (**2**) ATR72-60-KE, (**6**) CRJ1000-HE-300-5
H	(**4**) CRJ1000-KE, (**1**) CRJ1000-HE-620-5, (**7**) CRJ1000-HE-300-5
I	(**4**) CRJ1000-KE, (**4**) ATR72-60-KE, (**7**) CRJ1000-HE-300-5, (**1**) CRJ1000-HE-620-5

V. Conclusions & Recommendations

This article discusses a framework coupling hybrid-electric aircraft design with fleet assignment and airline network scheduling, incorporating aircraft off-design performance. The framework combines three parts; (1) a *Hybrid-Electric Aircraft Design Module*, including a powertrain and mission analysis model, (2) an *Off-design Analysis Module* which evaluates the maximum attainable power split ratio during cruise for different payload-range combinations and (3) a *Fleet Assignment & Scheduling Module* using dynamic programming to determine fleet composition and associated weekly schedule. The aforementioned modules are coupled through a clustering method, that uses passenger-distance data from the fleet assignment and scheduling to explore new HE aircraft designs. A subset of the Air Nostrum network was used as a case study. Original aircraft specifications were used to design hybrid-electric counterparts, spanning design ranges ranging from 300 km to 3000km and design power split ratios of 5% or 10%.

The baseline performance of the hybrid-electric aircraft, expectedly, showed the debilitating effect of the battery weight penalty on larger design ranges. However, consequently, the larger weight penalty results in relatively larger fuel burn reductions for equal reductions in mission length (compared to smaller design ranges). Thus, for short missions these aircraft achieve larger absolute fuel savings than aircraft sized for a smaller range. However, these fuel savings span a smaller domain of mission lengths. Furthermore, the combination of gas turbine operational limits and lower propulsive efficiency during climb of HE aircraft yields worse performance than their conventional counterparts on short missions. The larger the design range the greater the former effect.

Increasing the design power split ratio from 5% to 10% did not yield larger savings in terms of fuel at the payload-range combinations considered. The weight penalty from increasing the power split negated fuel savings for a large range of mission lengths. However, for a design power split ratio of 5% and progressively decreased design range, the aircraft demonstrating the largest fuel savings (for the largest domain of payload-range combinations) is not the

aircraft sized for the smallest range. In this study, the design range maximizing fuel savings is 620 km. This is of course case-specific, yet it highlights a non-linear relationship between design range and attainable off-design fuel savings.

The aforementioned conclusions are reflected in the fleet assignment and scheduling analysis for this specific network. In general, a fully hybrid-electric fleet yields a lower profit than a mixed-fleet or a fully kerosene fleet. Moreover, from a profit and emissions point of view, a fleet composed by aircraft with a smaller design power split ratio outperforms a fleet composed of aircraft with a larger power split ratio. In addition, reducing design range results is a smaller loss of profit than increasing design power split ratio, due to the relatively high demand on short routes. For this network, off-design cruise Mach numbers did not yield a profit benefit, or increase in captured demand.

When considering a mixed-fleet, it has been shown that a fleet composed of kerosene and hybrid-electric aircraft redesigned with a small design range can achieve savings in terms of CO_2 emissions in the order of 15%, whilst only experiencing a minimal reduction in total profit (1.35%). Total profit and total demand served could in fact be increased by attributing larger importance to emissions objective due to the nature of this network. Moreover, for both fully-hybrid and mixed fleets, modifying design range had a larger effect than design power split ratio on generating competitive hybrid-electric aircraft. These points highlight the importance of coupling aircraft design and strategic airline planning.

Future work will evaluate the possibility of using battery energy in other phases than cruise to potentially to increase fuel savings for very short missions. This may change the effect of design power split ratio. Additionally, it is relevant to consider airline networks with different demand-route distributions.

Acknowledgments

This article is based on the work performed during the MSc. thesis of Sofia Coelho Antunes[35]. The data used for the Air Nostrum case study has been obtained from OAG data under the license by University of Bergamo.

References

[1] Viswanathan, V., Epstein, A. H., Chiang, Y.-M., Takeuchi, E., Bradley, M., Langford, J., and Winter, M., "The challenges and opportunities of battery-powered flight," *Nature*, Vol. 601, No. 7894, 2022, pp. 519–525. https://doi.org/10.1038/s41586-021-04139-1.

[2] Wolleswinkel, R., de Vries, R., Hoogreef, M. F. M., and Vos, R., "A New Perspective on Battery-Electric Aviation, Part I: Reassessment of Achievable Range," *AIAA Scitech 2024 Forum*, American Institute of Aeronautics and Astronautics, 2024. https://doi.org/10.2514/6.2024-1489.

[3] de Vries, R., "Hybrid-Electric Aircraft with Over-the-Wing Distributed Propulsion: Aerodynamic Performance and Conceptual Design," Ph.D. thesis, Delft University of Technology, 2022. https://doi.org/10.4233/uuid:ef87dc11-e7b2-4726-a41f-28588d64c58d.

[4] Hoogreef, M. F. M., Bonnin, V. O., Santos, B. F., Morlupo, F., Wahler, N. F. M., and Elham, A., "Scalability Assessment of Hybrid-Electric Technology Application to Various Aircraft Classes - an Overview of Opportunities and Challenges," *Aerospace Europe Conference 2023 – 10th EUCASS – 9th CEAS*, 2023. https://doi.org/10.13009/EUCASS2023-260, publisher: EUCASS.

[5] Bonnin, V., and Hoogreef, M., "Exploration of Off-Design Performance for Hybrid Electric Regional Aircraft," *Journal of Aircraft*, 2024. https://doi.org/10.2514/1.C037893, to be published.

[6] Jansen, P., and Perez, R., "Coupled Optimization of Aircraft Family Design and Fleet Assignment for Minimum Cost and Fuel Burn," *12th AIAA Aviation Technology, Integration, and Operations (ATIO) Conference and 14th AIAA/ISSMO Multidisciplinary Analysis and Optimization Conference*, American Institute of Aeronautics and Astronautics, 2012. https://doi.org/10.2514/6.2012-5495.

[7] Taylor, C., and de Weck, O., "Coupled Vehicle Design and Network Flow Optimization for Air Transportation Systems," *7th AIAA ATIO Conf, 2nd CEIAT Int'l Conf on Innov and Integr in Aero Sciences,17th LTA Systems Tech Conf; followed by 2nd TEOS Forum*, 2007. https://doi.org/10.2514/6.2007-7710.

[8] Jansen, P. W., and Perez, R. E., "Coupled Optimization of Aircraft Design and Fleet Allocation with Uncertain Passenger Demand," *2013 Aviation Technology, Integration, and Operations Conference*, American Institute of Aeronautics and Astronautics, Los Angeles, CA, 2013. https://doi.org/10.2514/6.2013-4392.

[9] Roy, S., Moore, K., Hwang, J. T., Gray, J. S., Crossley, W. A., and Martins, J. R. R. A., "A Mixed Integer Efficient Global Optimization Algorithm for the Simultaneous Aircraft Allocation-Mission-Design Problem," *58th AIAA/ASCE/AHS/ASC Structures, Structural Dynamics, and Materials Conference*, American Institute of Aeronautics and Astronautics, 2017. https://doi.org/10.2514/6.2017-1305.

[10] Scheers, E., "Coupled hybrid electric aircraft design and strategic airline planning," Master's thesis, TU Delft, 2023.

[11] Zuijderwijk, N., "Study to the adaptation of electrified aircraft by regional airlines: using strategic airline planning and aircraft design," Master's thesis, TU Delft, 2022.

[12] Seoane Álvarez, M., "Assessment of the Climate Impact Mitigation Potential of Intermediate Stop Operations: A Dynamic Programming Approach," Master's thesis, TU Delft, Delft, The Netherlands, 2021.

[13] Noorafza, M., F. Santos, B., Sharpanskykh, A., L. Zengerling, Z., M. Weder, C., Linke, F., and Grewe, V., "Airline network planning considering climate impact: assessing new operational improvements," *Applied Sciences*, Vol. 13, No. 11, 2023. https://doi.org/10.3390/app13116722.

[14] Proesmans, P.-J., and Vos, R., "Airplane Design Optimization for Minimal Global Warming Impact," *Journal of Aircraft*, Vol. 59, No. 5, 2022, pp. 1363–1381. https://doi.org/10.2514/1.C036529.

[15] de Vries, R., Hoogreef, M. F. M., and Vos, R., "Range Equation for Hybrid-Electric Aircraft with Constant Power Split," *Journal of Aircraft*, Vol. 57, No. 3, 2020, pp. 552–557. https://doi.org/10.2514/1.C035734.

[16] Roskam, J., *Airplane design. Pt. 1. Preliminary sizing of airplanes.*, Roskam Aviation and Engineering, Ottawa, Kansas, 1985.

[17] Obert, E., "Drag polars of nineteen jet transport aircraft at Mach numbers M=0.40-0.60," Technical Report, 2013. (unpublished).

[18] Torenbeek, E., *Synthesis of subsonic airplane design*, Delft University Press, Delft, 1982.

[19] Thijssen, R., "Propeller Aircraft Design Optimization for Reduced Climate Impact," Master's thesis, TU Delft, 2022.
[20] Vos, R., and Farokhi, S., *Introduction to transonic aerodynamics*, volume 110, Springer, Dordrecht, 2015.
[21] Mattingly, J. D., Boyer, K. M., Haven, B. A., Heiser, W. H., and Pratt, D. T., *Aircraft engine design*, third edition ed., AIAA education series, American Institute of Aeronautics and Astronautics, Inc., Reston, Virginia, 2018.
[22] ICAO, "Annex 6 - Operation of Aircraft. Part I - International Commercial Air Transport," , Jul. 2018.
[23] Dallara, E., "Aircraft Design for Reduced Climate Impact," PhD Thesis, Stanford University, Feb. 2011.
[24] Bellman, R. E., "The Theory of Dynamic Programming," Tech. rep., RAND Corporation, Jan. 1954.
[25] Birolini, S., Antunes, A. P., Cattaneo, M., Malighetti, P., and Paleari, S., "Integrated flight scheduling and fleet assignment with improved supply-demand interactions," *Transportation Research Part B: Methodological*, Vol. 149, 2021, pp. 162–180. https://doi.org/10.1016/j.trb.2021.05.001.
[26] Wang, X., "Development of a dynamic operations optimization modelling framework," Master's thesis, TU Delft, Delft, The Netherlands, 2016.
[27] Pita, J. P., Adler, N., and Antunes, A. P., "Socially-oriented flight scheduling and fleet assignment model with an application to Norway," *Transportation Research Part B: Methodological*, Vol. 61, 2014, pp. 17–32. https://doi.org/10.1016/j.trb.2013.12.006.
[28] Kinene, A., and Birolini, S., "Optimization of subsidized air transport networks using electric aircraft," *Transportation Research Part B: Methodological*, Vol. 190, 2024, p. 103065. https://doi.org/10.1016/j.trb.2024.103065.
[29] Rubbrecht, P., "Development of an Airline Systems Simulation Program," Tech. rep., TU Delft, Delft, The Netherlands, 1989.
[30] Roskam, J., *Airplane design. Pt. 8. Airplane cost estimation: design, development, manufacturing and operating.*, Roskam Aviation and Engineering, Ottawa, Kansas, 1990.
[31] Jansen, P. W., and Perez, R. E., "Coupled Optimization of Aircraft Families and Fleet Allocation for Multiple Markets," *Journal of Aircraft*, Vol. 53, No. 5, 2016, pp. 1485–1504. https://doi.org/10.2514/1.C033646.
[32] Satopaa, V., Albrecht, J., Irwin, D., and Raghavan, B., "Finding a "Kneedle" in a Haystack: Detecting Knee Points in System Behavior," *2011 31st International Conference on Distributed Computing Systems Workshops*, 2011, pp. 166–171. https://doi.org/10.1109/ICDCSW.2011.20.
[33] Hoogreef, M., Zuijderwijk, N., Scheers, E., Proesmans, P.-J., and Santos, B. F., "Coupled Hybrid & Electric Aircraft Design and Strategic Airline Planning," *AIAA AVIATION 2023 Forum*, 2023. https://doi.org/10.2514/6.2023-3869.
[34] Ruijgrok, G., *Elements of airplane performance*, VSSD, 2009. 2nd edition lecture series with 'minor adjustments'.
[35] Coelho Antunes, S., "Optimizing hybrid-electric aircraft design and airline planning for efficient energy management and profitability through multidisciplinary coupling," Master's thesis, TU Delft, 2024. https://resolver.tudelft.nl/uuid:aa83b80b-bc9c-4c75-bde0-4a870c0996e2.
[36] Teeuwen, Y., "Propeller Design for Conceptual Turboprop Aircraft," Master's thesis, TU Delft, 2017.

Appendices

A. Powertrain Assumptions

The following appendix outlines the assumptions considered when designing the hybrid-electric powertrains. Table 12 outlines the assumptions of the gas turbine and Table 13 outlines the assumptions of hybrid powertrain overall.

Table 12 Gas turbine design variable assumptions retrieved from *Thijssen* [19]

Variable	$\Pi_{\text{compressor}}$	$T_{t,4}$	Π_{burner}	Π_{inlet}	Π_{nozzle}	$\eta_{\text{compressor}}$	η_{hpt} ‡	η_{lpt} ‡	η_{burner} ‡	η_{mH}	η_{mL} ‡
Value	14.3	1200	0.96	0.98	0.99	0.9	0.89	0.91	0.99	0.975	0.99

‡ hpt - High-pressure spool; lpt - Low-pressure spool; mH - Mechanical High-pressure spool; mL - Mechanical Low-pressure spool; burner - Combustion chamber.

Table 13 Hybrid powertrain properties. Estimates as of 2035, retrieved from *de Vries*.[3] and from *Scheers* [10]

Variable	**Value**	**Units**
Fuel Density, ρ_{fuel}	775[x]	[kg/m^3]
Specific Energy Fuel, e_{fuel}	11900	[Wh/kg]
Specific Energy Battery at pack level, e_{bat}	350	[Wh/kg]
Specific Power Battery at pack level, ep_{bat}	1000	[W/kg]
Energy Density Battery at pack level, ρ_{bat}	1000	[Wh/l]
SOC	20	%
Specific Power EM, ep_{em}	5940	[W/kg]
Efficiency GT, η_{gt}	40	[%]
Efficiency GB, η_{gb}	96	[%]
Efficiency EM, η_{em}	97	[%]
Efficiency PMAD, η_{pmad}	99	[%]
Maximum Efficiency Propeller, $\eta_{P,\text{max}}$	88†	[%]

† Used in combination with the flight Mach number to estimate the propeller efficiency η_P according to model by *Thijssen* [19]. Optimistic value, according to projections for the future [36].

B. Aircraft Designs

Table 14 Hybrid-Electric Aircraft On-design Analysis with battery energy density equal to 350 Wh/kg

Aircraft	**Power split ratio** [%]	$\mathbf{R_{design}}$ [km]	$\mathbf{M_{bat}}$ [t]	**MTOM** [t]		**b** [m]		M_f [t]	
				Value	Δ [%]	*Value*	Δ [%]	*Value*	Δ [%]
ATR72-600	5	1370	3.31	30.8	+25	32	+11.8	2.09	+3.7
ATR72-600	10	1370	8.10	41.3	+67.8	36.0	+25.8	2.67	+32.8
CRJ1000	5	1370	4.82	41.2	+17.9	30.6	+7.7	3.12	-40.1
CRJ1000	10	1370	12.3	57.4	+64.1	36.0	+26.7	3.95	-24.1
CRJ1000	5	300	1.49	31.8	-8.9	27.0	-5.1	1.34	-74.3
CRJ1000	5	450	1.71	32.6	-6.6	27.3	-3.9	1.53	-70.6
CRJ1000	5	620	2.22	34.0	-2.7	27.8	-2.1	2.22	-57.4
CRJ200	5	1370	2.64	21.8	+15.8	22.8	+7.0	1.70	-42.9

[x] https://exolum.com/wp-content/uploads/2021/06/AVIATION-KEROSENE-JETA1_issue-12.pdf